WORLD NUCLEAR ASSOCIATION

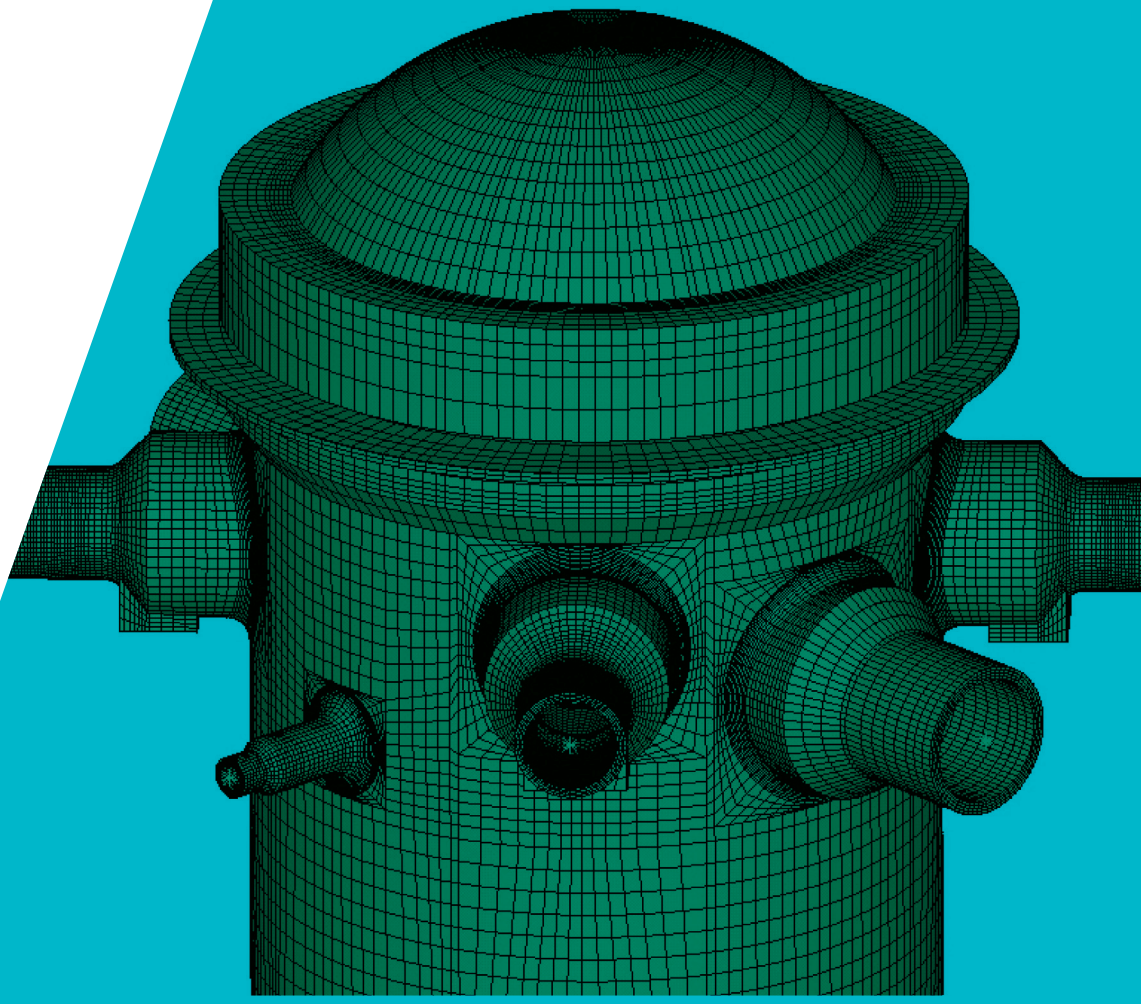

Non-Linear Analysis Design Rules

Part 2b: Assessment of Non-Linear Benchmark Results

Cooperation in Reactor Design Evaluation and Licensing – Mechanical Codes and Standards Task Force

Title: Non-Linear Analysis Design Rules
Part 2b: Assessment of Non-Linear Benchmark Results
Produced by: World Nuclear Association
Published: September 2020
Report No. 2020/010

Cover Photo: SPIC/SNERDI

Contributors to the Report

Technical Coordinator

Denis Pont, EDF (France)

David Clarkson, Rolls-Royce/University of Strathclyde (UK)

Project Coordinator

Mohammad Rababah, World Nuclear Association (UK)

Contributors

Benchmark 1:

Laurent Thiéry, Westinghouse (USA)

Chen Mingya, CGNPC (China)

Ludovic Jian, Naval Group (France)

Denis Pont, EDF (France)

Hyosub Yoon and team, Korea Electric Power Corporation-E&C (Korea)

Declan Gilmartin, Rolls-Royce (UK)

Hadagali Shivakumar, Prosim (India)

Roman Atroshenkov, Rosatom (Russia)

Ralf Trieglaff, TÜV NORD (Germany)

Hao Yu, SNERDI (China)

Benchmark 2:

David Clarkson, Rolls-Royce (UK)

Ludovic Jian, Naval Group (France)

Hyosub Yoon and team, Korea Electric Power Corporation-E&C (Korea)

Martin Beckert, Ralf Trieglaff and Sven Petersen, TÜV NORD (Germany)

Reviewers

Cécile Petesch, CEA/AFCEN (France)

Frédéric Beaud, EDF (France)

Hadagali Shivakumar, Prosim (India)

Nawal Prinja, Jacobs (UK)

Byung-Chan Na, World Nuclear Association (UK)

Foreword

The Cooperation in Reactor Design Evaluation and Licensing (CORDEL) Working Group was established in 2007 to promote the development of a worldwide regulatory environment where internationally standardized reactor designs can be widely deployed without major design changes due to national regulations.

The Mechanical Codes and Standards Task Force (MCSTF) of the CORDEL Working Group was set up in 2011 to collaborate with the Standards Development Organizations Board (SDO Board) and the Multinational Design Evaluation Program (MDEP) Codes and Standards Working Group (CSWG) on the international convergence of mechanical codes and standards related to the design of nuclear power plant components important to safety. The MCSTF's collaboration with regulators is now through the Committee for Nuclear Regulatory Activity (CNRA) of OECD/NEA. MCSTF has worked to date principally in three areas: qualification of non-destructive examination personnel; fatigue analysis and design rules; and non-linear analysis design rules.

In the area of non-linear analysis design rules, the topics identified by the MCSTF for investigation with a view to harmonized approaches are: review and comparison of the current code requirements in non-linear analysis for different failure modes (plastic collapse, plastic instability, local failure and buckling) and some degradation mechanisms (fatigue, plastic shakedown) (Part 1); definition of international benchmark problems to compare the existing non-linear analysis practices (Part 2a) and assessment of the benchmark results (Part 2b); and development of harmonized "recommended industrial practices" (Part 3).

This report is Part 2b of the series of reports on the non-linear analysis design rules.

In this report, the results of the two benchmarks for non-linear analysis of nozzles under pressure, thermal and piping loads are presented, compared, and assessed to highlight any differences which may emerge due to assumptions and interpretations made by international participants, even when the same design is being analyzed using similar software. Discussion is presented identifying the difficulties in these non-linear analyses and to give an insight into any differences observed in the submitted results.

The final goal of this activity is to offer recommendations for internationally harmonized practices in non-linear analysis which will be reported in Part 3.

Acknowledgement

The CORDEL Secretariat of the World Nuclear Association would like to convey its gratitude to colleague Richard Petrie for his diligent work in designing this report with great professionalism.

Abbreviations and acronyms

AFCEN: French Association for Design, Construction, and In-Service Inspection Rules for Nuclear Island Components

ASME: American Society of Mechanical Engineers

BNCS: ASME Board on Nuclear Codes and Standards

CGNPC: China General Nuclear Power Company

CORDEL: Cooperation On Reactor Design Evaluation and Licensing

KEPCO-E&C: Korea Electric Power Corporation-Engineering and Construction Company

EDF: Electricité de France

MCSTF: Mechanical Codes and Standards Task Force

NG: Naval Group

RCC-M: Design and Construction Rules for the Mechanical Components of PWR Nuclear Islands

RR: Rolls-Royce

SDO: Standard Developing Organization

SNERDI: Shanghai Nuclear Engineering Research and Design Institute

TÜV: TÜV NORD EnSys GmbH & Co. KG

WH: Westinghouse Electric Company LLC

WNA: World Nuclear Association

Technical nomenclature

CUF	Cumulative usage factor
FE	Finite element
FEA	Finite element analysis
FUF	Fatigue usage factor
HTC	Heat transfer coefficient
MCL	Main coolant line
SCL	Stress classification line
C_p	Specific heat capacity
E	Young's modulus
E_a	Young's modulus adopted for the fatigue cycle
E_c	Reference Young's modulus of the design fatigue curve
K_e	Fatigue plasticity correction factor (strain concentration factor)
K_e^{ther}	RCC-M thermal plasticity correction factor
K_e^{mech}	RCC-M mechanical plasticity correction factor
K_e^*	ASME III Record 17-225 proposed plasticity correction factor
P_b	Primary bending stress intensity
P_L	Primary local membrane stress intensity
P_m	Primary general membrane stress intensity
Q	Secondary stress intensity
R^*	Equivalent sphere radius
R_m	Ultimate tensile strength
$R_{p0.2}$	0.2% proof stress
S_{alt}	Alternating stress intensity
S_m	Allowable stress intensity
S_n	Primary-plus-secondary stress intensity range
S_p	Primary-plus-secondary-plus-peak (total) stress intensity range
S_p^{mech}	Total stress intensity range arising due to mechanical loads
S_p^{ther}	Total stress intensity range arising due to thermal loads
S_y	Monotonic yield strength
S_y^c	Cyclic yield strength
e	Element thickness
t	Time

$\Delta\varepsilon_{ep}$ Elastic-plastic equivalent strain range

κ Thermal diffusivity

λ Thermal conductivity

ρ Mass density

ν Poisson’s ratio

σ Stress

Contents

Tables

Figures

Executive Summary

This report is a part of series of reports aimed at developing a more harmonized approach in using non-linear analysis methods. Major pressure vessel and piping codes design rules, nuclear and non-nuclear, are based on linear elastic methods associated with stress classification in primary (for load control), secondary (for strain control) and peak stresses (for thermal shocks). This stress classification is easy to apply only in simple cases, such as cylindrical shell under axisymmetric quasi-static loads. When the geometry or the loads are more complex, such classifications are not applicable, so a large part of stress is considered as primary which is extremely conservative. In such cases, non-linear analysis methods are used. Comparison of these methods has shown that many different approaches are being used within the industry, giving rise to discrepancies in analysis and assessment of designs.

Following an initial comparison of non-linear analysis design rules in nuclear mechanical codes and standards (Part 1 of this series of reports), two benchmark problems were specified for two typical nuclear components (Part 2a of this series). The first benchmark problem was based on a large class 1 low alloy steel vessel nozzle under pressure and piping loads where the aim was to analyze elastic stress, plastic collapse, plastic instability and local failure. The second benchmark problem was based on a class 1 reinforced stainless steel piping tee under cyclic pressure and thermal loads to perform fatigue assessment. These two benchmarks consider only non-cracked components outside of creep regime.

This report (Part 2b) presents the comparison and assessment of the final results of two benchmarks. The objectives of this report are:

- to compare and assess the final results submitted by the participants to identify areas of the non-linear analysis methods where consensus appears to be emerging, and
- to identify areas where further discussions are needed to resolve differences in the non-linear analysis approach used by the analysts.

Assessment and findings of the benchmark results will be further developed in Part 3 in this series of reports on Non-Linear Analysis Design Rules, devoted to recommendations in support of international harmonization of non-linear analysis methods.

The benchmarks have been analyzed by ten international participants from China, France, Germany, India, Russia, South Korea, the UK and USA at various levels.

The assessment indicates that the differences observed among the results submitted by the participants arise due to three main causes:

- Modelling assumptions made by the analysts;
- Analysis and assessment methods adopted by the analysts;
- Differences in the design code rules.

In addition, this benchmark exercise has identified several areas where no guidance is provided in the design codes for the analysts. The following areas will be further developed to provide recommendations for industrial practices in non-linear analysis:

- How local stresses normal to the section are resolved;
- Selection and definition of the positioning of the section where stresses are being evaluated;
- More detailed guidelines about linearization procedures;
- Definition of the limits of the approach to analyze a 3D geometry with a 2D model;
- Selection of the location where strain is being monitored for strain-based methods to estimate limit loads;
- How to derive a true stress-strain curve from material data;
- Selecting the value of flow stress to be used for limit load;
- When to use full 3D analysis;
- How to reduce pessimism in limit load prediction by use of full 3D geometry model;
- Combination of transients for fatigue assessment;
- Calculation of K_e factor;
- Calculation of Fatigue Usage Factor (FUF).

1. Introduction

Following an initial comparison study of non-linear analysis design rules available in nuclear mechanical codes and standards [1], two non-linear analysis benchmark problems have been specified for two typical nuclear components [2]. The respective geometries defined for both benchmark problems are given in Figure 1 and Figure 2: a large class 1 low alloy steel vessel nozzle under pressure and piping loads for the first benchmark problem to analyze elastic stress, plastic collapse, plastic instability and local failure; and a class 1 reinforced stainless steel piping tee under cyclic pressure and thermal loads for the second benchmark problem to analyze fatigue and ratcheting margins.

The first benchmark is defined in five parts (1.0 Elastic Codified Approach, 1.1 Plastic Collapse and Local Failure, 1.2 Plastic Instability, 1.3 Piping Load Effect and 1.4 3D Effects). The second benchmark problem focuses on fatigue assessment and was done in two parts (2.0 Codified Elastic Fatigue and 2.1 Simplified Non-Linear Analysis).

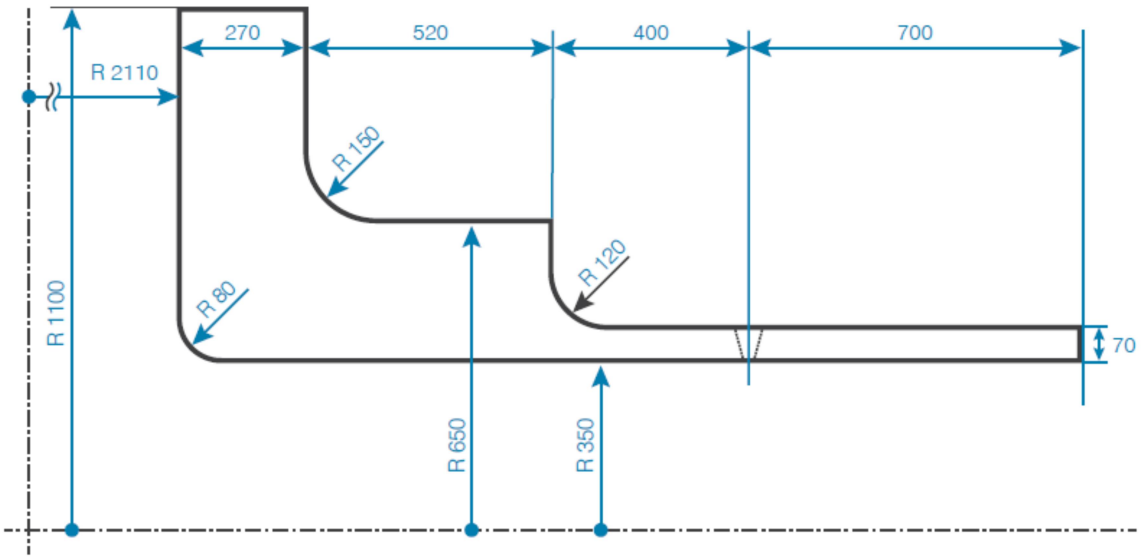

Figure 1. Benchmark 1 – Class 1 low alloy steel vessel nozzle

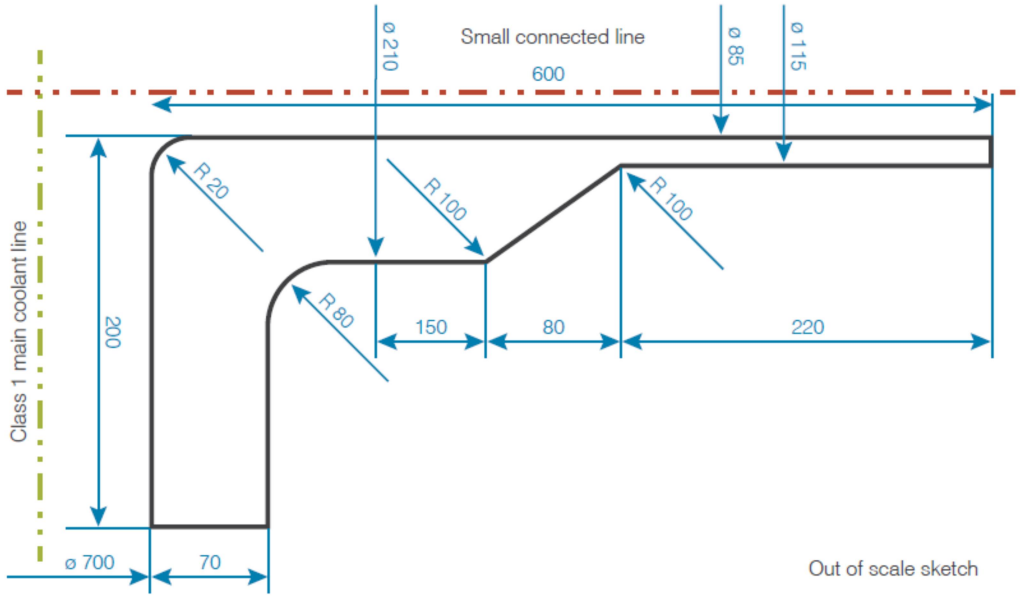

Figure 2. Benchmark 2 – Class 1 reinforced stainless steel piping tee

The benchmarks have been analyzed by ten international participants from China, France, Germany, India, Russia, South Korea, the UK and USA at various levels.

Table 1 below gives the full list of participants for the various steps of the benchmarks, along with the Finite Element Analysis (FEA) software used.

Table 1. List of participants and software used

Company	Software	Benchmark 1					Benchmark 2	
		1.0	1.1	1.2	1.3	1.4	2.0	2.1
		Elastic codified approach	Plastic collapse and local failure	Plastic instability	Piping load effect	3D effects	Codified elastic fatigue analysis	Fatigue simplified non-linear analysis
Westinghouse (USA)	ANSYS	✓	✓	✓	✓			
CGNPC (China)	ANSYS	✓	✓	✓	✓	✓		
EDF (France)	SYSTUS	✓	✓	✓	✓			
Naval Group (France)	SYSTUS						✓	✓
KEPCO-E&C (South Korea)	ANSYS & FASEM	✓	✓				✓	
Rolls-Royce (UK)	ANSYS & ABAQUS	✓	✓	✓	✓	✓	✓	✓
Prosim (India)	ABAQUS	✓	✓	✓	✓	✓		
Rosatom (Russia)	ABAQUS	✓	✓	✓	✓	✓		
TÜV Nord (Germany)	ABAQUS						✓	✓
SNERDI (China)	ANSYS	✓	✓	✓	✓	✓		

A pre-assessment of these results has been carried out and discussed at the Mechanical Codes and Standards Task Force (MCSTF) non-linear analysis workshop which was held on 4 August 2019 during the American Society of Mechanical Engineers (ASME) code week in Minneapolis, USA. The workshop was supported by Standard Developing Organization (SDO) Convergence Board. Following the workshop and further discussions at the MCSTF meetings on 2 September 2019 and 15 January 2020, the results were updated by participants.

The objectives of this report are:

- to compare and assess the final results submitted by the participants to identify areas of the non-linear analysis methods where consensus appears to be emerging,

and

- to identify areas where further discussions are needed to resolve differences in the non-linear analysis approach used by the analysts.

Assessments and findings of the two benchmark results are presented in this report and will be further developed in the next report, which will be devoted to recommendations in support of international harmonization of non-linear analysis methods.

It should be highlighted that the results and assessments presented in this report are obtained in the framework of the benchmark exercises and should not be directly compared to a design report that could be performed by the companies of the participants in the framework of an actual project. It is nevertheless expected that the participants follow their usual practice for such analyses.

2. Benchmark 1 – Comparison and assessment of results

Eight participants – Westinghouse (WH), CGNPC, EDF, KEPCO-E&C, Rolls-Royce (RR), ProSim, Rosatom and SNERDI –contributed results for Benchmark 1.

2.1 Benchmark 1.0: Elastic codified approach for P=17 MPa

The purpose of Benchmark 1.0 is to perform linear elastic stress analysis using an FEA on a 2D model to assess the typical codified rules (stress classification) given below:

- Primary stress intensity limits:
  - Membrane stress $P_m \leq S_m = 184$ MPa and $P_L \leq 1.5S_m = 276$ MPa
  - Combined membrane + bending stress (P_m or P_L) + $P_b \leq 1.5S_m = 276$ MPa
- Primary + secondary stress range limit:
  - Range of the sum of primary and secondary stresses < $3S_m = 552$ MPa (not considered in the present benchmark)
- Tri-axial stresses intensity limit:
  - Algebraic sum of the three primary principal stresses ($\sigma_I + \sigma_{II} + \sigma_{III}$) < $4S_m = 736$ MPa

The benchmark specification [2] requires membrane stress, bending stress and combined stress to be calculated at 12 sections, S1 to S12 (stress lines depicted in Figure 3). The selection of these sections is based on standard practices to capture the stress distribution in various areas. It is limited to the purpose of the benchmark exercise and does not constitute a reference for industrial studies.

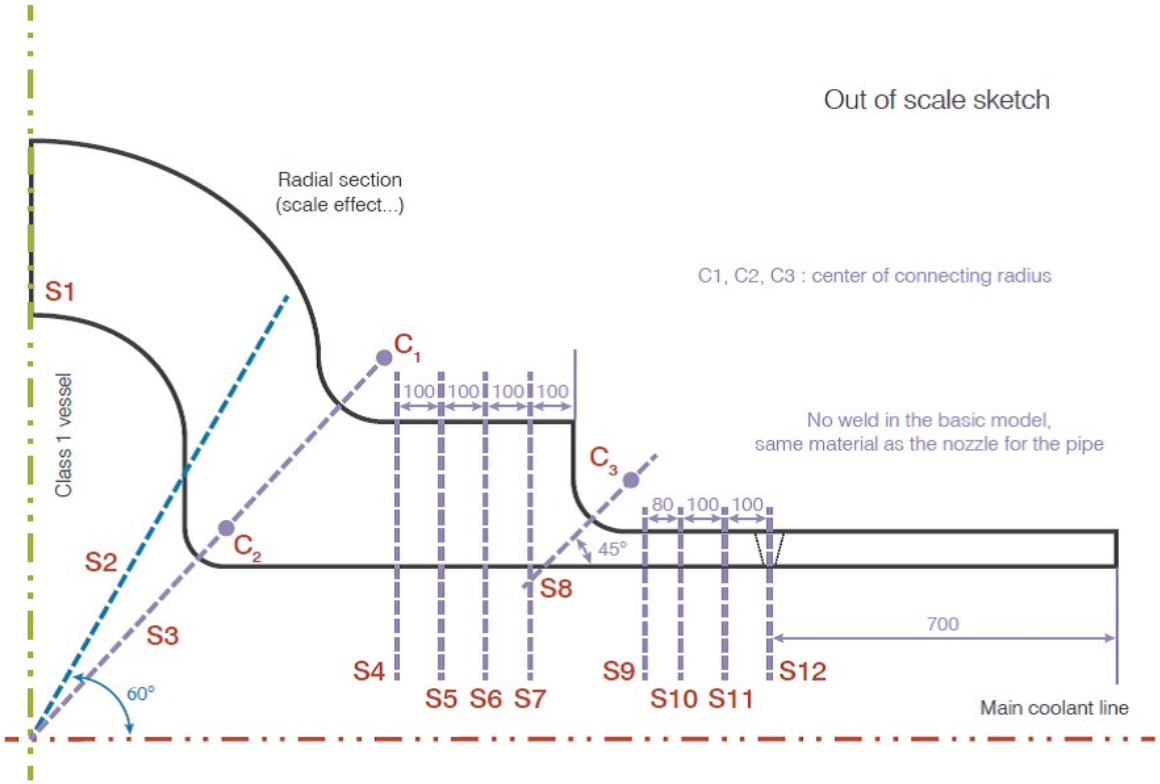

Figure 3. Benchmark 1 – Location of sections for post-processing

Figure 4, Figure 5 and Figure 6 present the membrane, bending and combined stresses predicted by the participants. Predicted values of $(\sigma_I + \sigma_{II} + \sigma_{III})$ and corresponding locations are shown in Table 2.

Stresses are evaluated across the section thickness by a linearization process. As for the primary stress intensity limits, only the primary stress profile is linearized. A full comparison of the stress profiles is outside the scope of the benchmark, as it is not meaningful with regards to the codified rules listed above.

Based on these stress values, some of the participants continued with the stress analysis to assess the codified rules listed above. Because not all results have been made available, the outcome of this analysis is not detailed in the present report. However, general considerations on stress classification (primary and secondary stresses) will be given in the assessment section for further discussion.

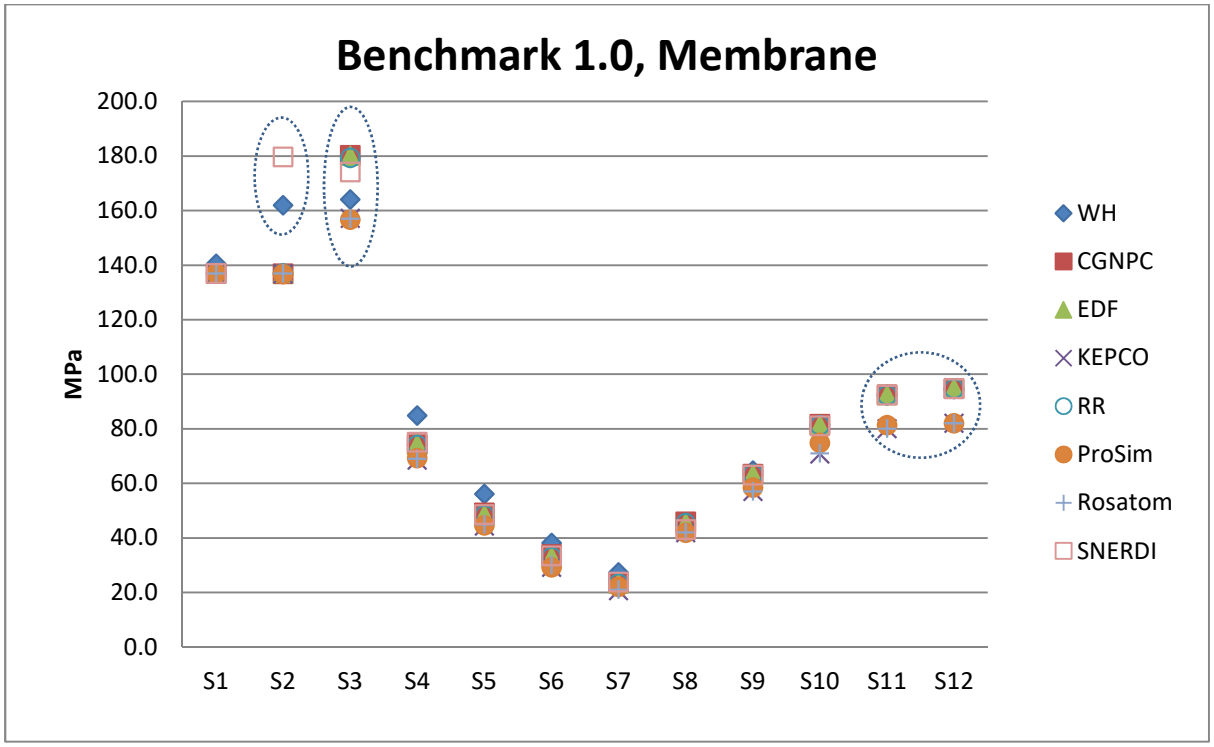

Figure 4. Benchmark 1.0 – Membrane stresses

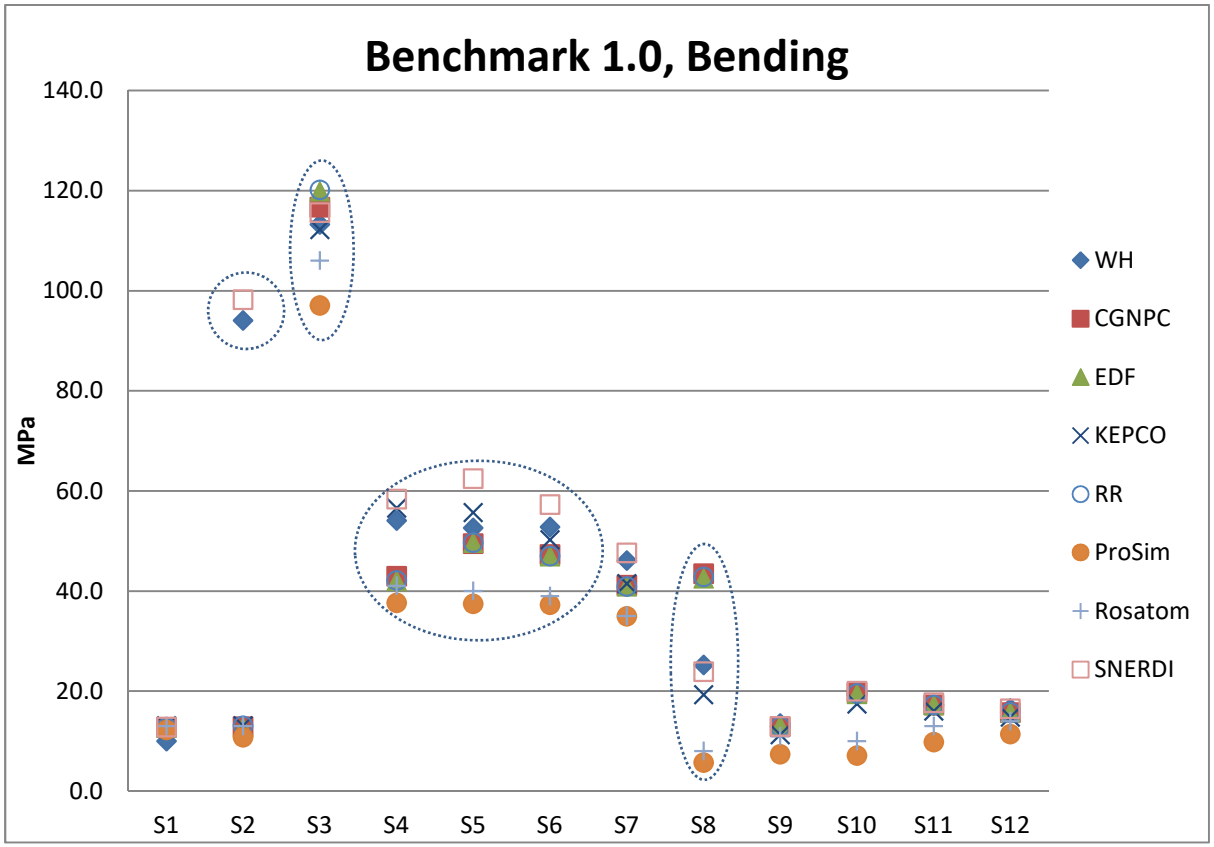

Figure 5. Benchmark 1.0 – Bending stresses

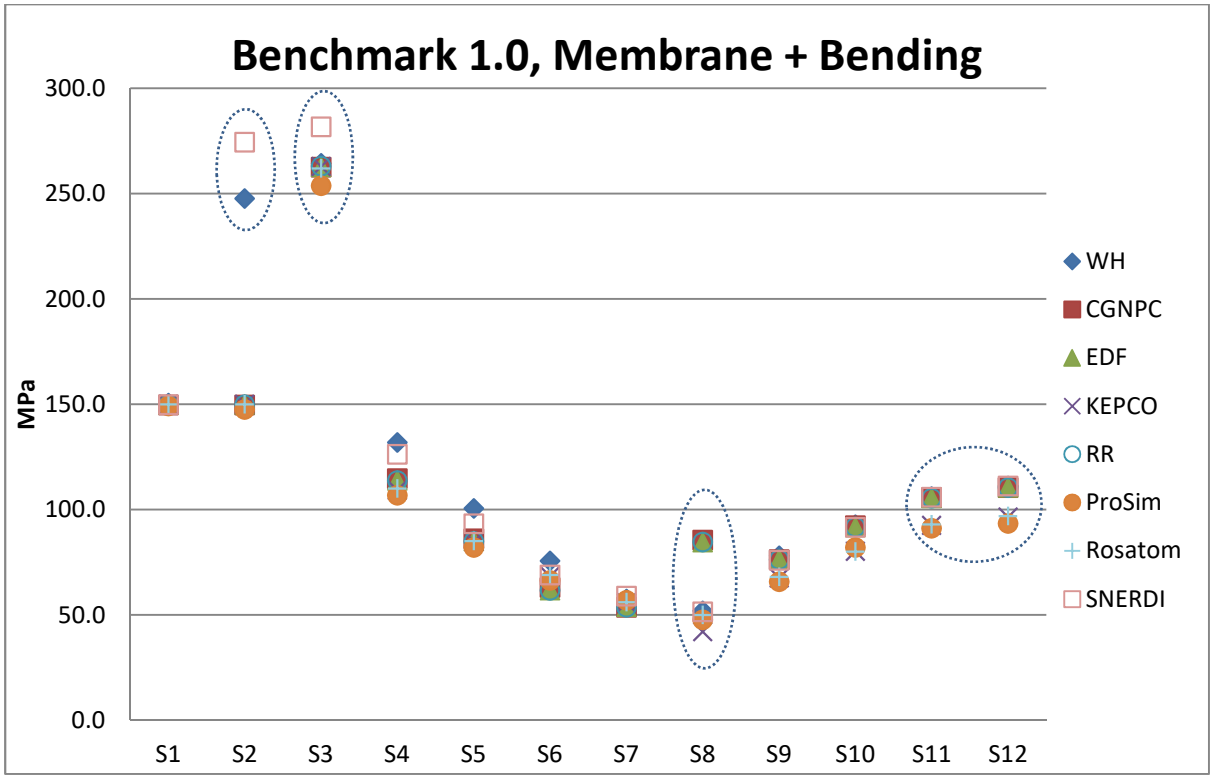

Figure 6. Benchmark 1.0 – Combined membrane + bending stresses

Table 2. Predicted values of ($\sigma_I + \sigma_{II} + \sigma_{III}$) and corresponding locations for Benchmark 1.0

Benchmark 1.0: $\sigma_I + \sigma_{II} + \sigma_{III}$ ($\leq 4S_m$ = 736 MPa)						
	max 1	location 1	max 2	location 2	max 3	location 3
CGNPC	249	S1	249	S2	240	S3
KEPCO	249	S1	249	S2	246/207	S3 (out/in)
WH	282	S2	267	S1	185	S3
EDF	249	S2	249	S1	242	S3
RR	249	S1	249	S2	210	S3
ProSim	249	S1 inner	250	S2 inner	234	S3 inner
Rosatom	378	S1	242	S2	255	S3
SNERDI	311	S2 outer	249	S1 inner	249	S1 outer

Figure 4 and Figure 6 show a good agreement of predicted membrane and combined stresses in the vessel and main coolant line outside of transition areas (sections S1, S4 to S7, and S9 to S12). The largest discrepancies are in sections S2, S3 and S8. It should be noted that S3 and S8 are inclined sections corresponding to the transitions from the vessel to the nozzle and from the nozzle reinforcement to the pipe respectively. The scatter of values in these sections may come from the FEA sensitivity to mesh refinement and section location in areas where stress concentrations and gradients are high. Care must also be taken to ensure how local stresses normal to the section are resolved. The two outliers in section S2 (Westinghouse and SNERDI values) would be explained by a difference in the positioning of the section. General recommendations should include the careful positioning of the sections used for post-processing stresses in discontinuity areas, as well as mesh refinement to properly capture stress gradients related to geometrical variations. Sensitivity analyses are a good way to control variations in the computed stresses.

There is a consensus that, away from the joint (reinforcement area), the membrane stress is predominant in the coolant line (around 80 to 100 MPa) and bending stress is much less (< 20 MPa). However, the variation in the level of stresses in the pipe away from the joint predicted by the participants is unexpectedly high for a linear elastic analysis. Differences in the application of boundary conditions at the pipe end may cause variations of membrane stress in sections S11 and S12. Differences could be resolved using analytic formulas in sections such as S12.

Variations in bending stress are believed to primarily come from the way bending stress values have been derived. Indeed, ProSim derived bending stress values from the difference between combined membrane + bending stresses and membrane stresses, which tend to minimize bending. It is thought Rosatom has performed a similar analysis, whereas other participants would have derived equivalent bending stress values from the linearized stress components.

Standards are usually based on Tresca equivalent stress for these kinds of analyses. It is assumed all participants have used Tresca criteria, but it could be worth confirming and possibly comparing stress components rather than equivalent stress in some locations.

Differences may also originate from the type of element, mesh refinement used in the model and the way stresses have been linearized, particularly bending stress. Type of element and mesh size should be sufficient to accurately simulate the behaviour of the component under applied loading. If the objective of an analysis is to obtain the membrane and bending stresses only, the analyst must question the need to employ refined meshes in finite element (FE) analysis because any peak stresses faithfully predicted by the FE method will be eliminated in the linearization procedure. None of the participants justified the use of the type of element or validated the mesh size.

By using solid continuum elements an analyst can, generally, obtain reasonably accurate stress distribution. Often such stress distributions vary non-linearly through the section. For assessment purposes, the stress distribution has to be 'linearized' to obtain the membrane and bending stresses which are in equilibrium with the loads being carried by the section. In this axisymmetric analysis, there are three direct stress and one shear stress components which can be linearized using one of the following five methods:

(i) All stress components are linearized;

(ii) Only direct stress components are linearized and the total shear stress at the surface is used;

(iii) Same as (ii) but averaged shear stress across the line is used;

(iv) Linearized axial and hoop components with total radial and shear stresses at surface;

(v) Same as (iv) but radial and shear stresses averaged across the line are used.

Note that shear stress on free surface should be zero, with a specific profile across the thickness of the section. None of the participants explained their linearization assumptions or justified the method. The need for more detailed guidelines about linearization procedures should be discussed with the participants.

For local failure, the sum of the three principal stresses has been predicted to be the highest in sections S1, S2 and S3 which are all in the vessel. Note that section S1 does not exist in real 3D geometry. Principal stress directions need to be confirmed by inspection of vector plots, but for axisymmetric components like vessels and pipes, one of the principal stresses is expected to be in the hoop direction. The use of a 2D axisymmetric model with twice the radius of the 3D vessel geometry leads to an overestimation of the axial stress in the actual vessel, with consequences on the equivalent stress depending on the location considered. A 3D model is used in Benchmark 1.4 which unfortunately does not include an elastic analysis for comparison with the 2D model. It is recommended that participants should discuss the limits of the approach to analyze a 3D geometry with a 2D model.

Not all the participants continued with the assessment of the codified rules, which requires consideration of the classification of membrane and bending stresses as primary or secondary loads depending on the type of loading and geometry with regards to the effect of structure deformation on the release of loading. Membrane stress arising from pressure or mechanical loads is generally considered as primary in uniform areas (general membrane stress P_m) and in discontinuity areas (local membrane stress P_L) in the respective equations required to satisfy the codified margins. The classification of bending stresses is subject to interpretation, as part of the equation on combined membrane + bending stress intensity limit (P_m+P_b or P_L+P_b where P_b is the primary bending stress). Future developments of the benchmark should consider sharing the practices in the classification of stresses between primary and secondary loads, referring to the rules set out in codes and standards, and discussing the use of non-linear analyses or other methods (e.g. 'Reduced Modulus') in support of the classification.

2.2 Benchmark 1.1: Vessel-Nozzle plastic collapse and local failure

The plastic collapse values based on S_y, double slope method and 0.5% strain are shown in Table 3 and Figure 7. The corresponding local failure values are listed in Table 4.

Table 3. Predicted plastic collapse load for Benchmark 1.1

Benchmark 1.1: Plastic collapse under pressure load			
Limit load pressure (S_y=303 MPa): C_{L1}			
	MPa	Location	Comments
CGNPC	37	-	
KEPCO-E&C	25	-	37.5 MPa without 1.5 margin
WH	38	-	
EDF	37	-	
RR	37	-	
ProSim	38	-	
Rosatom	34	-	
SNERDI	35	-	
Elastic-plastic (double slope): C_{L2}			
CGNPC	46	S1	
KEPCO-E&C	29	S3	43.5 MPa without 1.5 margin
WH	46	S1	

EDF	46	near S2 Vessel	36 MPa with elastic-plastic stress-strain curve set at S_y=303 MPa instead of $R_{p0.2}$=383 MPa for 0.2% plastic strain
RR	44	S3	
ProSim	42	-	
Rosatom	38	F4	
SNERDI	48	Inner shell adjacent to nozzle	
Elastic-plastic (max strain 0.5%): C_{L3}			
CGNPC	42	S3	
KEPCO-E&C	28	S3	42 MPa without 1.5 margin
WH	41	-	
EDF	42	S3	34 MPa with elastic-plastic stress-strain curve set at S_y=303 MPa instead of $R_{p0.2}$=383 MPa for 0.2% plastic strain
RR	42	S3	
ProSim	40	-	
Rosatom	41	F5	
SNERDI	43	Nozzle inner	

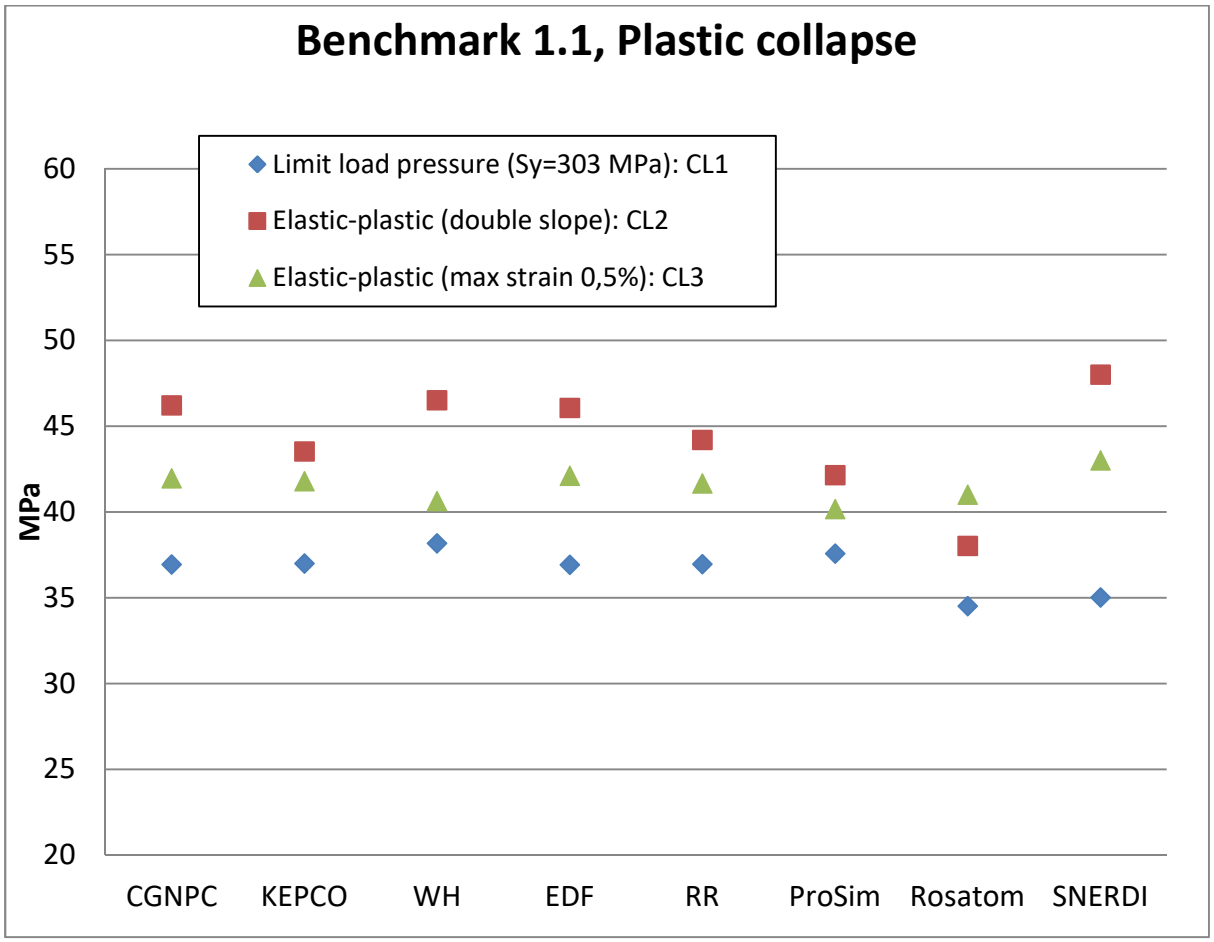

Figure 7. Benchmark 1.1 – Plastic collapse

Table 4. Local failure predictions for Benchmark 1.1

	Benchmark 1.1 for elastic-plastic (0.5%)					
	$\sigma_I + \sigma_{II} + \sigma_{III}$ inner					
	max 1 (MPa)	location 1	max 2 (MPa)	location 2	max 3 (MPa)	location 3
CGNPC	582	S1	582	S2	466	S4
KEPCO-E&C	635	S1	634	S2	563	S3
WH	556	S1	543	S2	347	S4
EDF	587	S1	587	S2	501	S4
RR	583	S2	577	S1	457	S4
ProSim	574	S1	573	S2	328	S3
Rosatom	586	S9	540	S10	435	S11
SNERDI	822	S2	637	S1	439	S3
$\sigma_I + \sigma_{II} + \sigma_{III}$ outer						
	max 1 (MPa)	location 1	max 2 (MPa)	location 2	max 3 (MPa)	location 3
CGNPC	639	S1	639	S2	578	S3
KEPCO-E&C	579	S1	579	S2	459	S4
WH	659	S1	579	S2	477	S3
EDF	651	S1	651	S2	589	S3
RR	634	S1	628	S2	542	S3
ProSim	605	S1	603	S2	557	S3
Rosatom	856	S6	720	S7	675	S8
SNERDI	585	S1	447	S4	352	S3

There is a good agreement in the values of the limit load pressure (C_{L1}) predicted by the participants. There is general consensus that the limit load C_{L1} for this benchmark is 37 MPa and that values predicted within 5% of margin should be acceptable. All results lie within this error margin. Limit loads are predicted by FEA and tend to be upper bound values. The limit loads predicted by the other two methods (double slope C_{L2} and max 0.5% strain C_{L3}) show similar trends, with C_{L3} indicating marginally lower values. It is clear from the results that the limit load is primarily influenced by the FEA method used to calculate it. Note that these methods depend on the location where strain is being monitored. Some participants have based it on section S1 which is not in the real 3D geometry. Collapse loads based on section S3 would be more realistic overall, but it does not affect the conclusions of the present exercise aimed at comparing results among 2D models. It would be interesting to compare the non-linear results with the elastic analyses, and to discuss the consistency of codified margins.

In addition to the above limit load estimates, local failure was also assessed through the sum of the three principal stresses. The results shown in Table 4 indicate the highest stresses are in sections S1, S2 and S3. These are similar to the linear elastic analysis results shown in Table 2 but the magnitudes are much higher in line with the level of pressure, indicating

build-up of hydrostatic stress which is not controlled by the plastic flow rules used in the FEA codes. Note that section S1 does not exist in the real 3D geometry. At sections S2 and S3, higher stress occurs on the outer surface indicating that the outer surface is more vulnerable to de-cohesion failure (but bi-axial stress state on the outer surface might mitigate the risk).

Note 1: In metal plasticity, two yield criteria are used: von Mises and Tresca. Normally, FEA codes prefer von Mises to Tresca but design codes like ASME are based on Tresca. According to the Tresca criterion, yielding occurs when the maximum shear stress reaches the specified yield stress. For Tresca calculation, the contribution of the maximum shear stress is twice the difference between the maximum and the minimum principal stresses. The von Mises criterion reduces three dimensional stresses to a single equivalent stress, also known as the von Mises stress, which is then compared against the specified yield stress. Participants have not explained the yield criteria that have been used to obtain the limit loads. The yield criteria used in the analysis codes are normally based on von Mises stresses.

Note 2: The benchmark had specified the stress-strain curve to be used. Normally, such detailed material stress-strain curves may not be available for all temperatures. Therefore, it is important to discuss in the next step how to derive a true stress-strain curve from material data like E, ν, $R_{p0.2}$, S_y and R_m.

Note 3: One of the participants (EDF) has shown that replacing the S_y value (stress at 0.2% plastic strain) of 383 MPa with 303 MPa (to be consistent with S_y used in C_{L1} flow stress) changes C_{L2} value from 46 MPa to 36 MPa, which is consistent with the C_{L1} result. It also changes C_{L3} value from 42 MPa to 34 MPa. The value of flow stress to be used for limit load analysis needs to be discussed further in Part 3.

It is recommended that the participants should discuss the following points:

(i) Value of flow stress to be used for C_{L1} method, consistent with elastic-plastic methods: $R_{p0.2}$ or S_y;

(ii) Comparison of C_{L1}, C_{L2} and C_{L3} methods with linear analyses;

(iii) Yield criteria: von Mises or Tresca;

(iv) Use of engineering stress-strain or true stress-strain curves;

(v) Method to derive stress-strain curves from material data such as E, ν, $R_{p0.2}$, S_y and R_m;

(vi) Influence of type of elements and mesh size on limit load and plastic collapse;

(vii) Location of strain to be monitored to determine the collapse load.

2.3 Benchmark 1.2: Vessel-Nozzle plastic instability

The plastic instability predictions under pressure load based on flow stress, 5% strain and 10% strain are shown in Table 5 and Figure 8.

Table 5. Plastic instability under pressure load results for Benchmark 1.2

Benchmark 1.2: Plastic instability under pressure load			
	MPa	Location	Comments
Limit load Pressure $(S_y+R_m)/2$: C_{l1} (S_y = 303 MPa)			
CGNPC	56	-	
WH	53	-	
EDF	51	-	
RR	51	-	
ProSim	46	-	
Rosatom	48	-	
SNERDI	51	-	
Elastic-plastic (5%): C_{l2}			
CGNPC	56	S3	
WH	58	S3	
EDF	55	S3 inner	44 MPa with elastic-plastic stress-strain curve set at S_y=303 MPa instead of $R_{p0.2}$=383 MPa for 0.2% plastic strain
RR	57	S3	
ProSim	58		
Rosatom	58		
SNERDI	56	Nozzle inner	
Elastic-plastic (10%): C_{l3}			
CGNPC	60	S3	
WH	58	S3	
EDF	60	S3 inner	47 MPa with elastic-plastic stress-strain curve set at S_y=303 MPa instead of $R_{p0.2}$=383 MPa for 0.2% plastic strain
RR	63	S3	
ProSim	66	-	
Rosatom	65	-	
SNERDI	65	Nozzle inner	

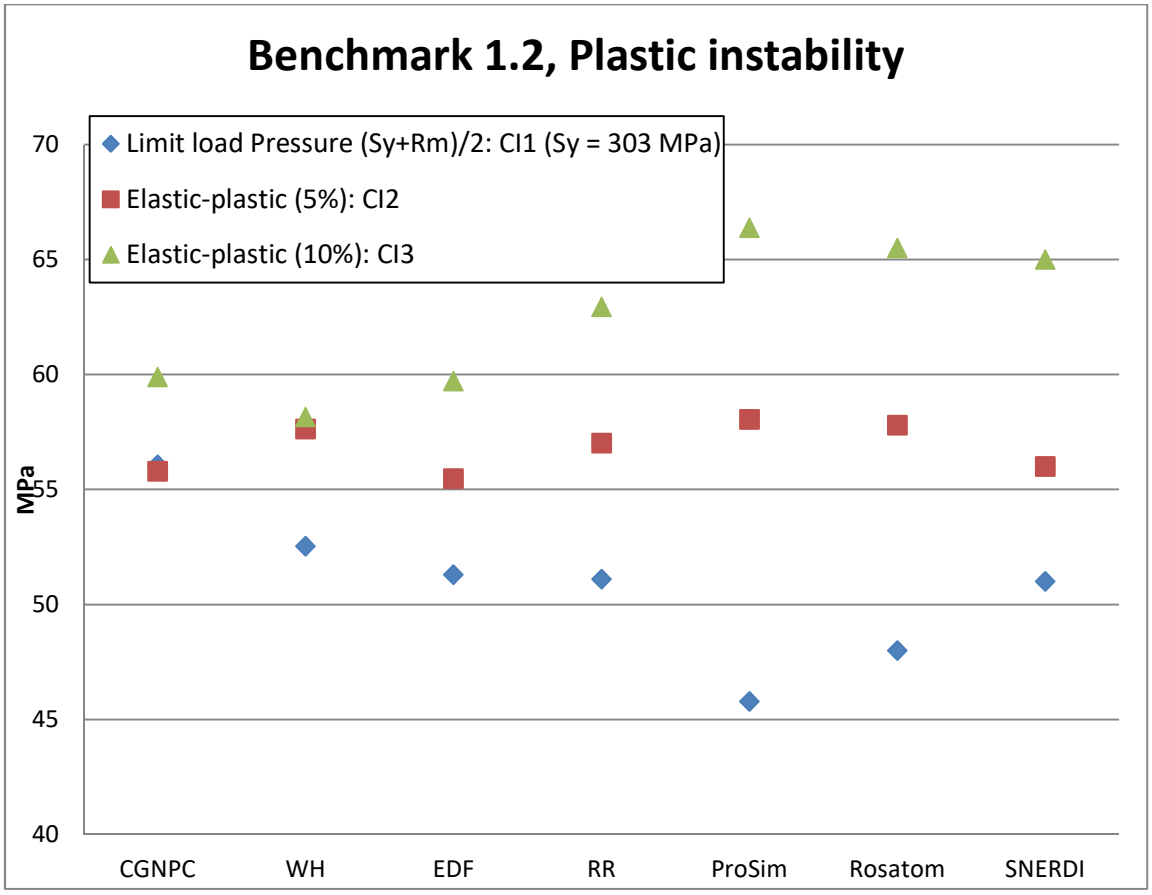

Figure 8. Benchmark 1.2 – Plastic instability

C_{l1} values range from 46 MPa to 56 MPa. As expected, the results indicate that the 10% strain criterion gives higher plastic instability loads compared to those predicted by the 5% strain limit. Since the value of $(S_y+R_m)/2$ is less than the stress at 5% strain, it is expected that the $(S_y+R_m)/2$ criteria will predict the lowest plastic instability load and therefore, it is a function of the material characteristic represented by the stress-strain curve. In this case, it appears that $C_{l1} < C_{l2} < C_{l3}$. Any participant predicting C_{l2} as the highest load should re-examine their results.

It should be noted that strain-based criteria are influenced by the location of the strain. All the participants have identified S3 as expected. Another factor that influences the results is the value of the yield stress used to calculate the flow stress. One of the participants (EDF) has shown that changing the S_y value (stress at 0.2% plastic strain) from 383 MPa to 303 MPa (to be consistent with S_y used in C_{l1} flow stress) changes C_{l2} value from 55 MPa to 44 MPa. The value of flow stress to be used for limit load analysis needs to be discussed.

It is recommended that participants should discuss the following:

(i) Value of flow stress to be used for C_{l1} method: $(R_{p0.2} + R_m)/2$ or $(S_y + R_m)/2$;

(ii) Location of the strain being monitored to determine the limit load;

(iii) Comparison of C_{l1}, C_{l2} and C_{l3} methods with linear analyses.

2.4 Benchmark 1.3: Piping load effect on Benchmarks 1.0 and 1.2

The purpose of this benchmark is to predict the effect of additional piping load on the membrane and bending stresses (Benchmark 1.0) and on the plastic instability (Benchmark 1.2). The membrane, bending and combined stress plots at the 12 sections are shown in Figure 9, Figure 10 and Figure 11 respectively. The plastic instability estimates are given in Table 6.

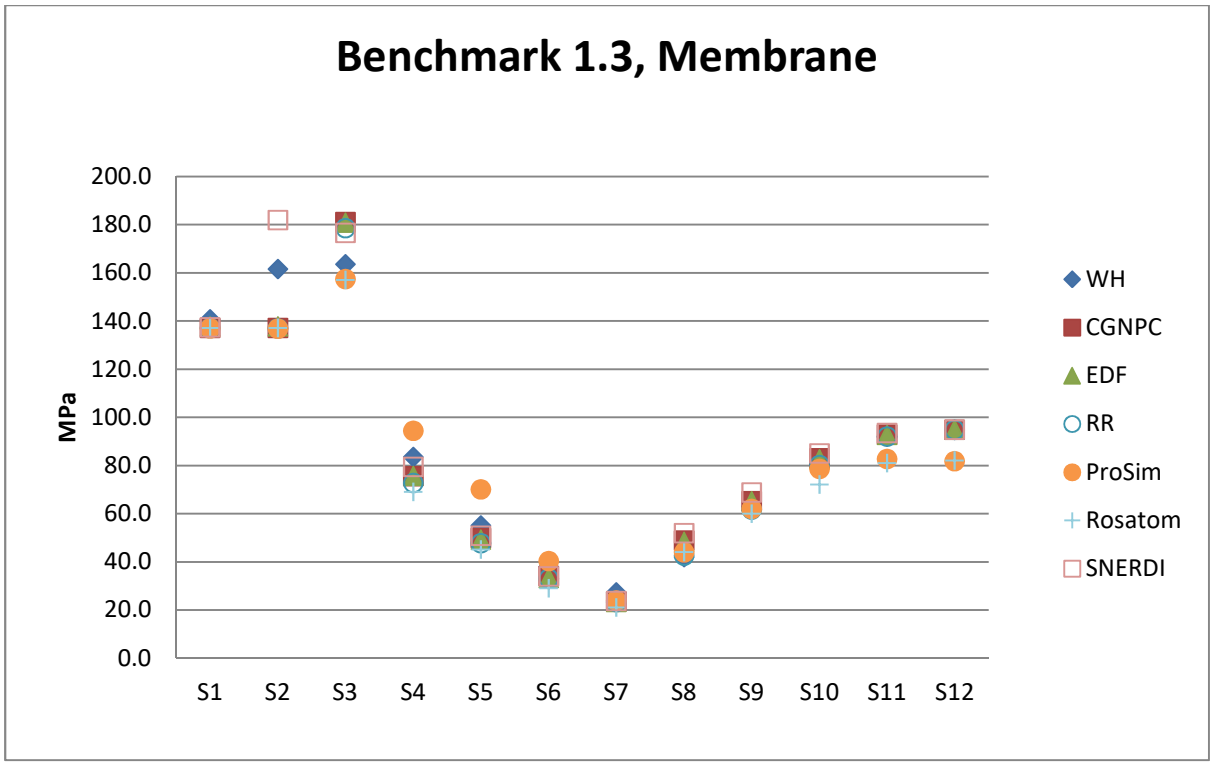

Figure 9. Benchmark 1.3 – Membrane stresses

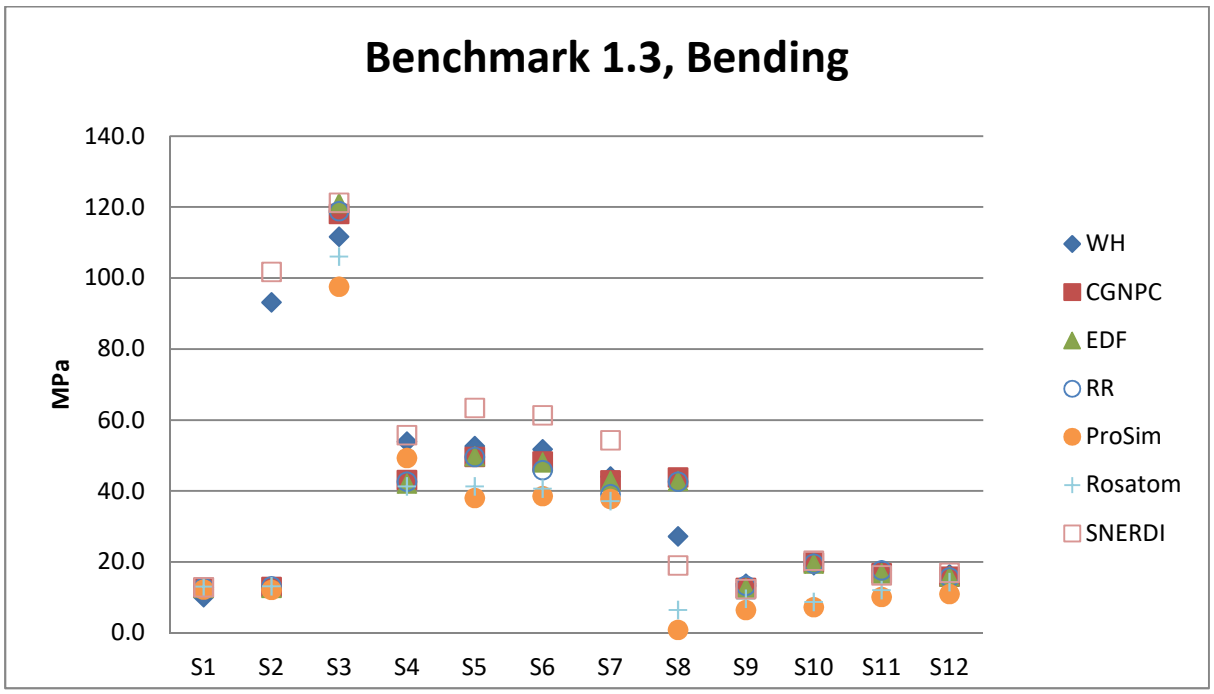

Figure 10. Benchmark 1.3 – Bending stresses

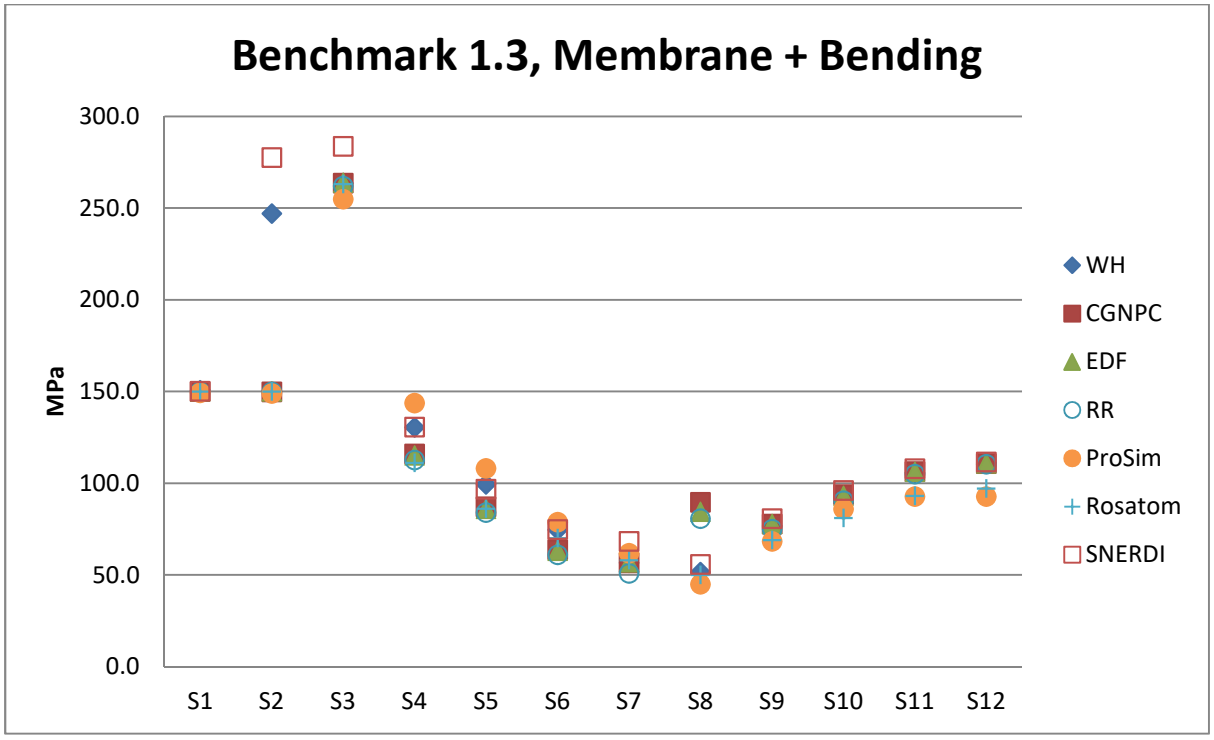

Figure 11. Benchmark 1.3 – Combined membrane + bending stresses

Table 6. Piping load effect on plastic instability for Benchmark 1.2

Benchmark 1.3: Piping load effects			
	MPa	Location	Comments
Limit load $(S_y+R_m)/2$: C'_{l1}			
CGNPC	51		
WH	53		
RR	51		
ProSim	44		
Rosatom	48		
SNERDI	51		
Elastic-plastic (5%): C'_{l2}			
CGNPC	56	S3	
WH	58	S3	
RR	57	S3	
ProSim	59		
Rosatom	58		
SNERDI	56	Nozzle inner	
Elastic-plastic (10%): C'_{l3}			
CGNPC	60	S3	
WH	58	S3	
RR	63	S3	
ProSim	67		
Rosatom	65		
SNERDI	65	Nozzle Inner	

Only axial load on the pipe equal to $1x10^6$ N has been applied in this example. This axial load only generates less than 10 MPa of general membrane stress in the coolant line and insignificant additional bending stress. Therefore, the stress plots in Figure 9, Figure 10 and Figure 11 are almost identical to those without pipe axial load in Figure 4, Figure 5 and Figure 6. As a result, the plastic instability loads shown in Table 6 are almost same as those without the pipe load given earlier in Table 5.

This particular benchmark has not added much value to the non-linear analysis methods. For the exercise to be meaningful, participants should consider a higher piping load, potentially including bending.

2.5 Benchmark 1.4: 3D effects on Benchmarks 1.1 and 1.2

The main purpose of this benchmark is to analyze the 3D geometry as it is and ascertain the difference made by analyzing it using a 2D axisymmetric model to assess plastic collapse and plastic instability (Benchmarks 1.1 and 1.2).

Five participants have submitted the results predicting the limit loads C''_{L1} and C''_{L3} based on S_y and max strain of 0.5%, and also the plastic instability load C''_{I1} and C''_{I2} based on flow stress $(S_y+R_m)/2$ and max strain of 5%. The results are presented in Table 7.

Table 7. Benchmark 1.4 3D effect on Benchmarks 1.1 and 1.2

Benchmark 1.4		
3D effects on Benchmark 1.1: plastic collapse		
	MPa (3D)	MPa (2D) (Benchmark 1.1)
Limit load S_y: C''_{L1}		
CGNPC	40	37
RR	40	37
ProSim	46	38
Rosatom	33	34
SNERDI	41	35
Elastic-plastic max strain 0.5%: C''_{L3}		
CGNPC	31	42
RR	30	42
ProSim	35	40
Rosatom	30	41
SNERDI	49	43
3D effects on Benchmark 1.2: plastic instability		
	MPa (3D)	MPa (2D) (Benchmark 1.2)
Limit load $(S_y+R_m)/2$: C''_{I1}		
CGNPC	56	56
RR	55	51
ProSim	42	46
Rosatom	48	48
SNERDI	49	51

Elastic-plastic max strain 5%: C"$_{l2}$		
CGNPC	55	56
RR	55	57
ProSim	62	58
Rosatom	65	58
SNERDI	52	56

Compared with the 2D results, the limit load based on S_y is increased from 37 MPa to an average of 45.5 MPa. This shows that the assumptions made to represent a real 3D geometry as a 2D axisymmetric geometry are pessimistic. Higher and more realistic limit loads can be obtained if real 3D geometry is modelled. The differences in the results could be due to all the factors previously discussed for Benchmarks 1.1 and 1.2.

For the limit load based on 0.5% max strain criteria, all participants except one indicated lower load when employing a full 3D model. Again, this could be due to the location where the strain is being monitored.

The plastic instability limit load C''$_{l1}$ using the flow stress of $(S_y+R_m)/2$ shows slightly lower values and C''$_{l2}$ based on the 5% max strain limit shows slightly higher values. The differences are all within 10%.

It can be concluded that the 3D model has confirmed that the limit loads and plastic instability loads obtained from the 2D model are within a 10% margin.

Participants should discuss the following:

(i) When to use full 3D analysis;

(ii) The limits of the approach to analyze a 3D geometry with a 2D model.

3. Benchmark 2 - Comparison and assessment of results

Four participants – Rolls-Royce (RR), Naval Group (NG), Korea Electric Power Corporation-E&C (KEPCO-E&C) and TÜV NORD (TUV) – have contributed results for benchmark 2.0.

3.1 Benchmark 2.0: MCL Nozzle – Codified elastic fatigue analysis

The main purpose of benchmark 2.0 is to perform a fatigue assessment of an auxiliary piping nozzle fabricated from Type 316L austenitic stainless steel (Figure 12) using elastic FEA results. In this benchmark, two quantities are derived: the plasticity correction factor, K_e, and fatigue usage factor (FUF) at the inner and outer surface of ten locations. The assessment locations are defined by the stress classification lines (SCLs), numbered S20-S29 as shown in Figure 13. The elastic fatigue analysis is to be performed in accordance with two code rules, ASME BPVC Section III [3] and AFCEN RCC-M Volume B [4] for three transients: Transient 1 (T1), Transient 2 (T2) and their combination Transient 1+2 (T3).

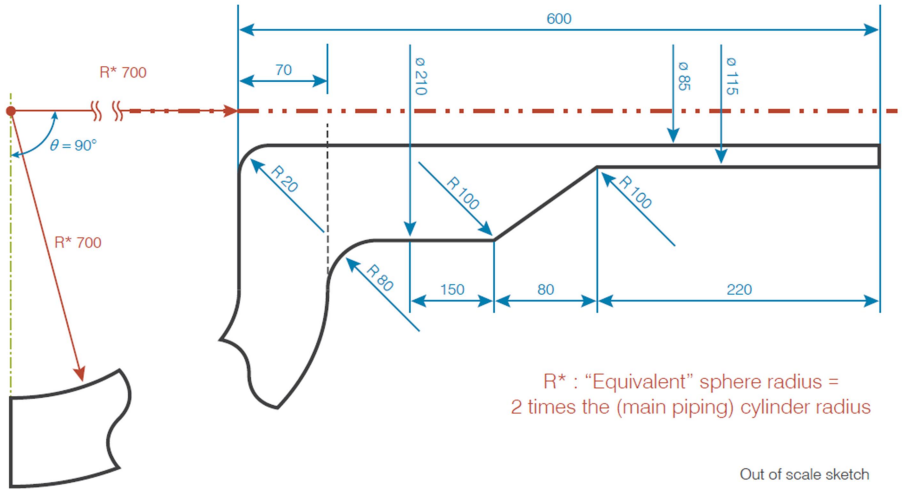

Figure 12. Benchmark 2 – Geometry of Class 1 auxiliary piping nozzle (Type 316L)

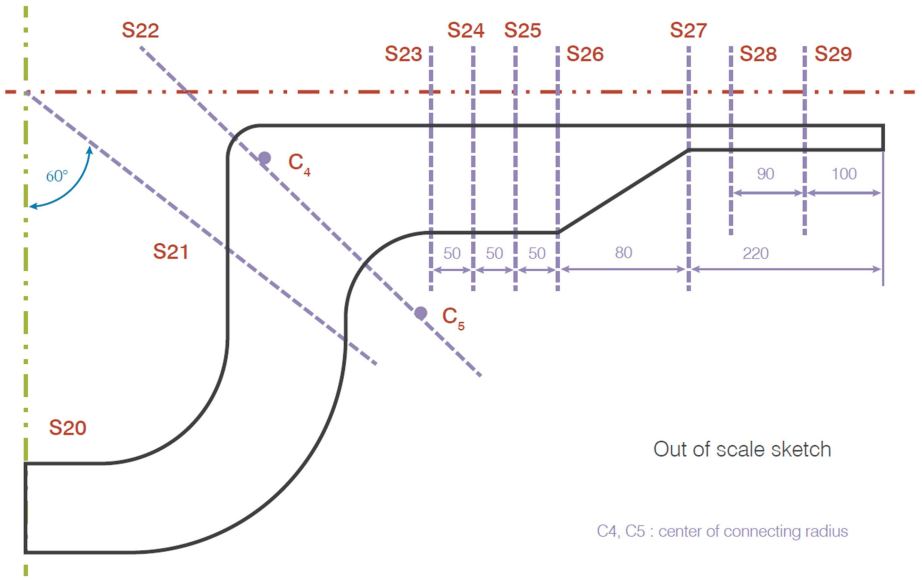

Figure 13. Benchmark 2 – Locations selected for fatigue evaluation

Participants were asked to discuss the following:

(i) Type of elements and mesh size;

(ii) Use of 2D axisymmetric model for a 3D geometry;

(iii) For each transient, the selection of an appropriate time-pair, to accommodate the phase difference between S_n and S_p. Comparison between the two participants (RR and Naval-Group) has been performed to show these differences;

(iv) Method used to calculate RCC-M K_e for Transient 2;

(v) Method used to calculate the cumulative usage factor (CUF) for the transient combination;

(vi) Use of alternative K_e methods (ASME Code Case N-779, Record 17-225, etc.)

The mesh refinement for this problem is dictated by Transient 2, where the nozzle experiences a very sharp 150°C thermal shock in 1s. Due to the definition of an infinite convective heat transfer coefficient (HTC) between the nozzle and contacting fluid, this closely approximates a step-change in metal temperature. Accordingly, the selection of an appropriate mesh size to capture the thermal shock stresses was seen as an important consideration by the participants. An estimate of the thermal penetration depth after 1s is given by $d = \sqrt{3\kappa t} \cong 3.68\ mm$ and therefore the time step discretisation must also be small enough (around 0.1s) to capture the peak surface stresses.

One participant (NG) established their mesh by estimating the minimum element thickness required on the inner layer as a function of the thermal properties, $e < \sqrt{\frac{6\lambda\nu\Delta T}{\rho C_p}} \cong 1.65.$

Another participant (RR) performed a mesh optimization study by comparing the peak thermal hoop stresses obtained from FEA to the analytical thermal stress solution for a straight pipe subjected to an arbitrary fluid temperature change on its inner surface, which closely approximates the behaviour at locations S20 and S29 (Figure 14 and Figure 15).

A mesh sensitivity study considering element thicknesses of 0.5, 1, and 1.65 mm up to 5 mm from the internal surface was also performed to determine the influence on S_p and S_n (Figure 16 and Figure 17). The element thickness on the inner layer was found to have little influence on Transient 1, but was of higher importance for Transient 2. Overall, the consensus amongst participants was that an inner element thickness of 1mm is sufficient to capture closely the peak thermal shock stresses at reasonable computational cost without excessive error. Additionally, the choice of mesh was concluded to have negligible impact on S_n, which is largely insensitive to mesh density.

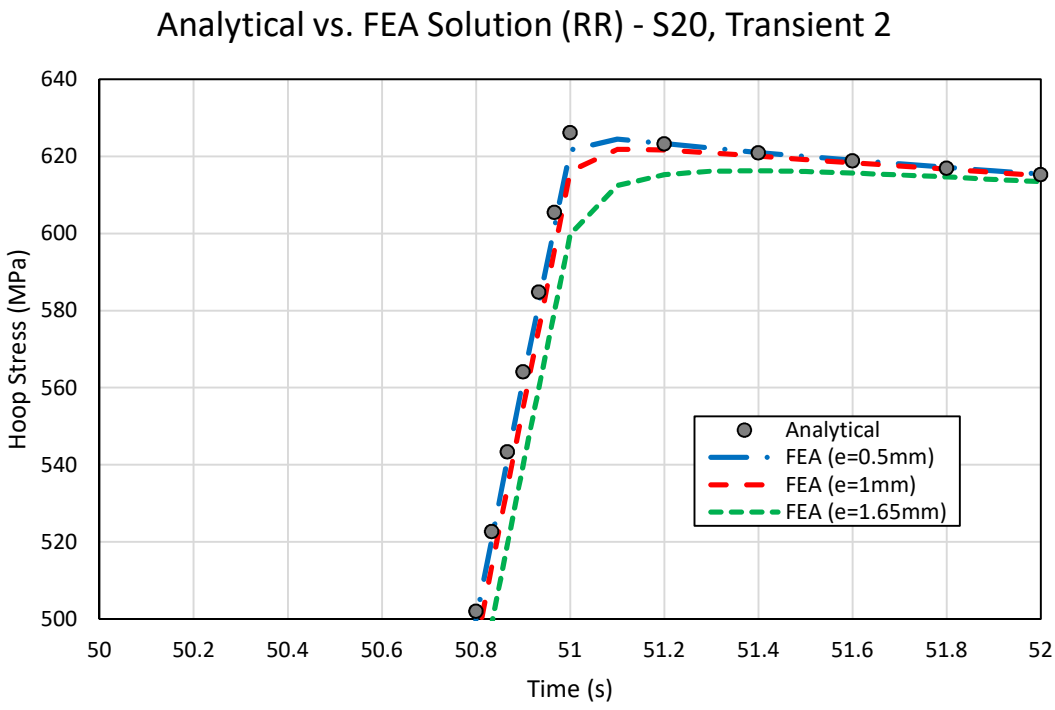

Figure 14. Analytical vs FEA solution – S20, Transient 2

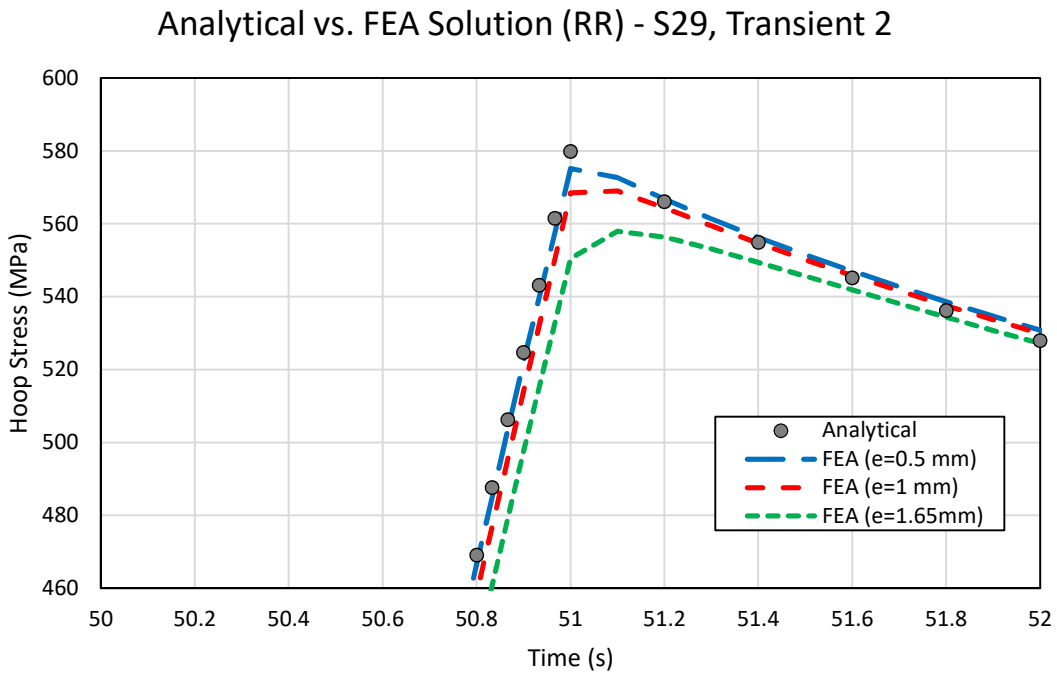

Figure 15. Analytical vs FEA solution – S29, Transient 2

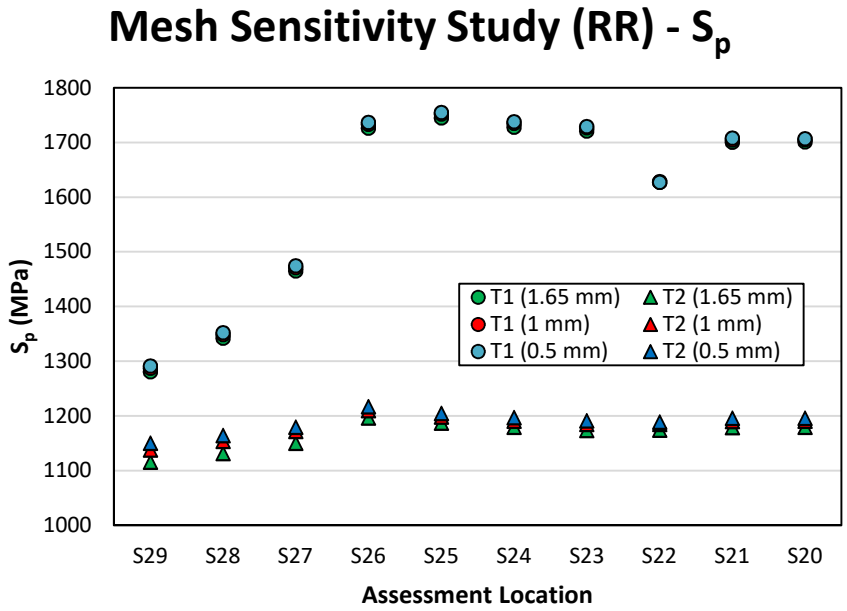

Figure 16. Mesh sensitivity study – effect on S_p

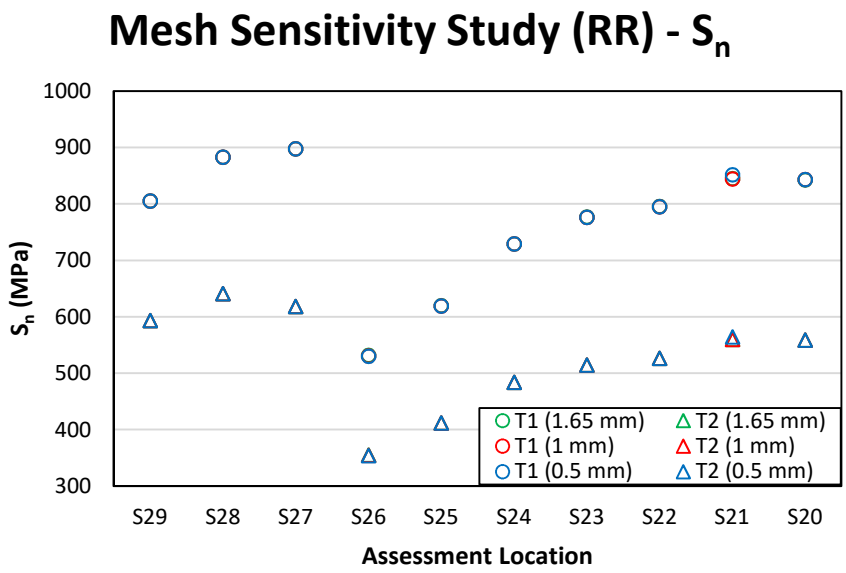

Figure 17. Mesh sensitivity study – effect on S_n

The validity of 2D axisymmetric FE analysis was also an important point of discussion between participants for this benchmark problem. The adoption of an equivalent sphere radius, R*, for the shell section (main coolant line) of the 2D model is intended to mimic the pressure-induced stresses that would be expected in a full 3D FE model of the main coolant line, remote from the intersection. However, it was acknowledged that this 2D idealization is still not expected to capture entirely the stress distribution of a detailed 3D model, specifically because a 2D axisymmetric model cannot capture the ovalization effect of two intersecting cylinders. Therefore, it would be expected that the largest divergence in results between 2D axisymmetric and 3D analyses might occur around the crotch corner region (S22). This potential loss in accuracy was however deemed acceptable given the significant reduction in computational expense that is achievable from 2D axisymmetric analyses. This benchmark problem is also dominated by thermal loads and therefore this was deemed not to be such a significant issue.

Figures 18 to 41 summarize the K_e and FUF results calculated by each participant on the inner and outer surfaces of the assessment locations.

Tables 8 to 14 provide the tabulated results submitted by each participant. A general trend from inspection of the plots for Transient 1 is that the K_e value obtained by using ASME Section III, Appendix XIII-3450 is almost double the value obtained from the RCC-M B-3234.6. This is the major contributor to the higher FUFs predicted by ASME III. This difference in the FUF results between ASME III and RCC-M is more pronounced for Transient 2, especially in the nozzle region.

Inspection of Figures 16 to 23 show that there is good overall agreement in the trend of predicted K_e and FUF for the case of Transient 1. The largest discrepancies were found to be in section S20 situated in the main coolant line remote from the intersection, and sections S26 and S27 at the juncture between the nozzle and branch piping. It is expected that equivalent results should be achieved at both S20 and S21 since both these sections are

representative of a thick-walled cylinder in an equivalent 3D model of the assembly. However, some differences in the K_e and FUF results were observed by some participants between these locations. At S21 and S22 in particular, care needs to be taken to ensure that stresses are resolved with respect to a cylindrical coordinate system defined locally to the SCL. There is a consensus that for Transient 1, the highest FUF is achieved in the nozzle (S23-S25) and main coolant line (S20, S21) regions, with the critical location determined to be S25 for both ASME III and RCC-M by most participants.

Figures 24 to 31 show generally good agreement of the trend in the K_e and FUF results calculated for Transient 2. In this case, there were found to be different discrepancies depending on the code calculation method. For ASME III, the largest differences in K_e and FUF were found to be in the nozzle region (S23-S26). This is attributed to the fact that $3S_m < S_n < 3mS_m$ at these locations, and therefore even small differences in S_n can lead to larger differences in K_e due to the sharp increase in the Appendix XIII-3450 K_e equation in this region. On the other hand, the RCC-M K_e and FUF results were in better agreement since differences in S_n had a relatively smaller impact, as the RCC-M B-3234.6 K_e^{ther} equation does not sharply increase in this region. The consensus amongst participants was that the highest K_e and FUFs according to ASME III occur in the branch pipe (S27-S29) and main coolant line (S20-S21). Comparatively, the nozzle experiences less damage according to ASME III, since due to the characteristics of Transient 2, a lower S_n is achieved which does not necessitate a maximum K_e penalty. In contrast, two participants (RR and NG) found that the highest K_e and FUF according to RCC-M are at the nozzle crotch corner (S22). The reason for this is due to the effect of the pressure drop, which contributes to a higher mechanical stress intensity range, S_p^{mech}, at this location, which must be addressed explicitly in RCC-M calculations. However, it was recognized that significant differences could arise in the RCC-M fatigue results for Transient 2 depending on analyst assumptions, which are highlighted later in this report.

Figures 32 to 39 show the K_e and FUF results calculated for the combination of Transient 1 and 2 (T3). Participants agreed that for ASME III, the location of maximum FUF is in the main coolant line (S20-21). This is due to this region experiencing the highest surface stresses and achieving a maximum K_e factor for both T1 and T2. For RCC-M, there was some difference in the location of maximum FUF among participants and this was found to be due to the calculation method employed. Two participants (RR and NG) agreed that the location of highest FUF according to RCC-M is the nozzle crotch corner (S22), whilst the other participants (TUV and KEPCO-E&C) determined the highest FUF to be in the main coolant line (S20-21) and branch pipe (S27-29), respectively. In the case of both ASME III and RCC-M, the highest FUF for the transient combination T3 corresponded closely to the highest FUF for T2. Whilst T2 is less damaging on a per-cycle basis compared to T1, it has a much greater influence on the FUF calculated for T3 due to its high number of cycles (800). It is important to note however that the transient combination methods of ASME III and RCC-M differ somewhat which may also explain some of the differences observed in the results. Additionally, as noted previously, the method used to account for fluctuating mechanical loads in RCC-M calculations can also have a significant effect.

A number of FE analysis assumptions were considered as having potential effects on the fatigue analysis results. One example is slight variations in the peak and valley time points used to determine S_p and S_n, which can be influenced by the choice of time-step discretization adopted within the FE software. The level of refinement in the transient thermal

FE solution may also have an effect. Additionally, differences in the mesh size adopted by participants close to the inner surface may also have an effect on S_p, especially due to the infinite HTC specified. Finally, the effect of significant figures/rounding in the reported results was identified as another source of possible differences. Overall, these factors only had a minor effect on S_p at the inner surface, which was generally within 1-2% between participants.

The choice of linearization method may also have an influence on S_n. Neither ASME III nor RCC-M provides explicit guidance on stress linearization and it is left to the judgement of the analyst. Generally, linearization of all stress components tends to be the most prevalent within industry for fatigue analysis since this is often the default option utilized by most FE-based linearization tools. Other codes such as ASME BPVC Section VIII, Division 2 [5] provide guidelines for performing stress linearization within Annex 5A, based on the recommendations outlined in Welding Research Council (WRC) Bulletin 429 [6]. WRC-429 states that bending stresses need only be computed for components that possess valid bending, namely the axial and circumferential component stresses. This recommendation may not always be appropriate for thick-walled structures however. The difference between these two methods is only expected to be significant in situations where the radial through-wall stresses are non-negligible, which is often limited to thick-walled vessels/piping or transition regions. None of the participants disclosed their choice of linearization method, though it was assumed that linearization was performed for all unique stress components owing to the similar trend observed in the reported S_n values. The choice of linearization method and its relevance to fatigue calculations is to be explored in further detail in the following report (Part 3).

It is however acknowledged that whilst the stress ranges (S_p and S_n) between participants were similar overall, even minor differences can have a significant 'knock-on effect' for downstream fatigue calculations. The reason for this is twofold. Firstly, it is due to the high non-linearity of the design fatigue curve in the low-cycle regime, where even a small difference in stress amplitude can result in a rather dramatic difference in fatigue usage; secondly, slight differences in S_n may lead to potentially large differences in K_e (e.g. in the range $3S_m < S_n < 3mS_m$ for ASME III), which can also have a dramatic effect on the fatigue usage.

At an early stage of this project, it was discussed whether a common set of stress histories should be provided to all participants for performing the fatigue analysis. It was however agreed that the purpose of this benchmark should be to compare the methods and assumptions adopted for both the FE stress analysis and subsequent fatigue calculations. The main argument against directly providing the stress information was that it would effectively eliminate a fundamental aspect of the engineering problem, and therefore would not be representative of the challenges faced by industry practitioners in realistic scenarios.

A number of analyst assumptions in the fatigue analysis procedure had the potential to produce a much larger impact on the results and warrant further discussion.

One circumstance that can arise is the possibility of the primary-plus-secondary (P+Q) stress time history being out-of-phase (lagging) the total stress time history. This is because the P+Q stress is highly dependent on the section thickness, and can have a much slower stress response than that of the total stresses. This can be especially significant for thicker

sections, such as the nozzle (S23-S26) and main coolant line (MCL) (S20-S21) assessment locations. Consequently, the peak and valley time points respectively forming S_p and S_n do not normally coincide. This is important since the alternating stress is a function of both K_e and S_p, where K_e is a function of S_n and the allowable stress intensity, S_m. Performing cycle counting per ASME III, Appendix XIII-2400 ensures maximization of S_p, but ASME III does not state as an explicit requirement that S_n need also be independently maximized. On the other hand, the fatigue evaluation procedure of RCC-M B-3234.5 requires that S_n be independently maximized. Therefore, this represented a possible factor that could introduce ambiguity in the analysis results. The choice of whether or not to independently maximize S_p and S_n can have an obvious impact on the calculated value of S_{alt} and therefore the participants were asked to clarify which method was adopted in their calculations. Three participants (RR, NG and TUV) performed the evaluation based on independently maximized S_p and S_n, to enable a more conservative K_e factor calculation. Another participant (KEPCO-E&C) adopted a different approach, wherein several peak-valley pairs were assessed within a time window and the pair that produced the maximum value of S_{alt} (and therefore FUF) was selected based on consideration of S_p, K_e, and the elastic modulus adjustment factor, E_c/E_a. This is illustrated in Figure 42. In this approach, the time points associated with the maximum S_{alt} need not necessarily coincide with peaks or valleys in the total or P+Q stress history, but often lie somewhere between the points that form the maximum S_p or S_n. Thus, the major distinction between these two approaches is that in the former, S_p and S_n are determined based on two distinct pairs of time points corresponding to their respective maxima and minima, whereas in the latter approach they are evaluated based on the same unique pair of time points. This was determined to be a major source of difference between the K_e and FUF values reported by participants.

A second major source of difference identified by two participants (RR and NG) is that the RCC-M results for Transient 2 could differ significantly depending on the methodology adopted for calculating S_p^{mech} and S_p^{ther} in accordance with RCC-M B-3234.6.

Two options are permissible in RCC-M B-3234.6 for evaluating S_p^{ther}. The first option is to evaluate S_p^{ther} based on the stress history generated from thermal loads alone. The second option is to determine S_p^{ther} based on the difference between the S_p and S_p^{mech} established by the peak and valley points that form S_p. The latter approach can lead to less conservative results especially when mechanical and thermal loads vary out-of-phase as in the case of Transient 2. The differences between these two approaches were investigated by both participants and were very significant for Transient 2 (Figure 43 and Figure 44), where direct calculation of S_p^{ther} results in a large increase in the FUF. This was found to be most significant for the nozzle crotch corner (S22), which experienced a 46% increase in the FUF using this approach, and actually became the fatigue critical location. This is because the nozzle experiences the highest mechanical stress intensity range, S_p^{mech}, due to the pressure drop, which is only fully captured by adopting the first option for calculating S_p^{ther}. This leads to a higher weighting applied to the more conservative K_e^{mech} factor in RCC-M B-3234.6, and consequently gives a higher value of S_{alt} and FUF. Therefore, the difference in calculation approach for S_p^{ther} was also concluded to be an important consideration by participants when performing fatigue calculations to RCC-M, especially for transients where fluctuating mechanical loads are significant and out-of-phase with the thermal loads.

It should be noted that for RCC-M, the weighted-average effect of the two corrections (K_e^{mech} and K_e^{ther}) is already 'built in' to the value of alternating stress intensity (S_{alt}) calculated based

on the RCC-M B3234.5 (c) 1.(b) equation. If the practitioner wants to reduce the combined effect of both K_e corrections to a single value for comparing with other code K_e methods then it is as simple as taking $[(2*S_{alt}) / S_p] * E_a/E_c$. This is valid for all plasticity correction methods that involve more than a single correction factor, not just RCC-M. It is therefore already implicit from the way S_{alt} is calculated for all codes. Two participants (RR and NG) therefore opted to report an equivalent RCC-M K_e factor, $K_{e,eq} = [(2*S_{alt}) / S_p] * E_a/E_c$ to represent the actual plasticity correction for Transient 2, rather than reporting only K_e^{ther}. This also explains some differences in the reported K_e values for RCC-M in this case.

Another important source of differences in results concerns the method adopted for the cross-combination of Transients 1 and 2 (T3), which differs between ASME III and RCC-M. The ASME III fatigue methodology is based on time instant combinations. In other words, the critical times within all transients where the stress achieves an extreme (peak or valley) are directly combined together, usually in a worst-case combination. On the other hand, the RCC-M methodology combines transients together rather than individual instants in time. In this approach, for a pair of transients (e.g. T1 and T2), the maxima and minima in both transients are determined; then, in combining these four instants together, the maximum stress amplitude out of any two of the four instants is defined as *fictive transient 1*, whilst the lesser stress amplitude formed by the remaining two instants is defined as *fictive transient 2*. The usage factor of a transient pair is then calculated as the sum of the usage factors associated to fictive transient 1, fictive transient 2, and any remaining sub-cycles. Benchmark 2.0 represents the case of two transients with no '*outside pairs'*. That is, no fatigue cycles are formed which consist of a peak in one transient and a valley from another separate transient. Therefore, the instant and transient combination methods of ASME III and RCC-M lead to identification of the exact same cycles for the cross-combination of T1 and T2. However, there is one very important but often overlooked difference concerning the application of the K_e factor, which can also lead to differences in the fatigue usage results even for a transient combination containing only inside pairs. For a given transient combination, the RCC-M K_e factor is calculated from the maximum value of S_n. It is then required to apply this maximum K_e factor to both fictive transients 1 and 2 and to any remaining sub-cycles. This differs to ASME III, where a distinct K_e factor is applied to each specific time combination. Therefore, this represents another potential source of difference between the code fatigue evaluation methods when considering transient combinations.

Finally, a further comment raised by participants concerned the application of an alternative ASME III K_e factor, which, at the time of writing, has received approval from the ASME Board on Nuclear Codes and Standards (BNCS) for publication as an ASME Section III Code Case (Record17-225 [7]). There was an interest to observe how this new K_e factor, denoted K_e^* in [8], compared with the other K_e factors analyzed. One participant (RR) investigated this difference for Benchmark 2.0 and the K_e and FUFs obtained are summarized in Figures 45 to 54. Overall, the new ASME III K_e^* factor exhibited a similar trend to the RCC-M K_e factor, and accordingly the FUFs calculated using this new approach are much more closely aligned to RCC-M compared with the standard ASME III, Appendix XIII-3450 approach. However, there were found to be some cases where more significant divergence can occur between K_e^* and the RCC-M K_e factors, which can arise depending on the loading condition. This is to be discussed in the next step (Part 3) of this project report.

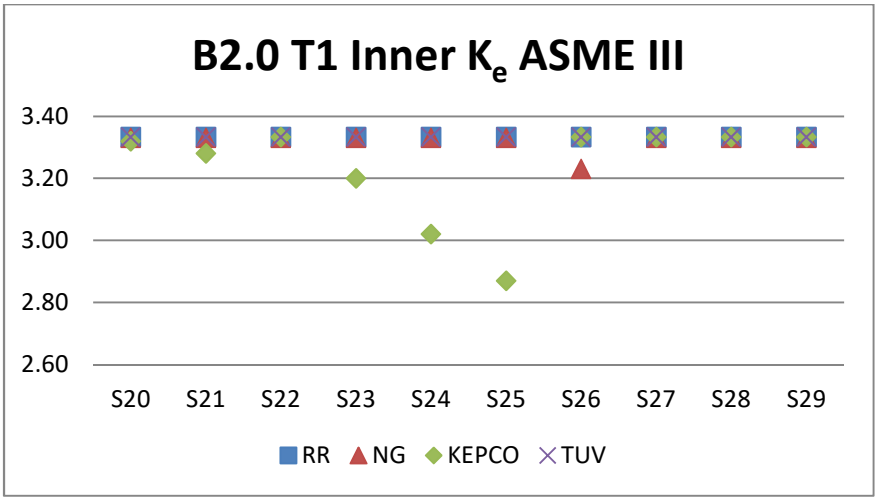

Figure 18. Benchmark 2.0 T1 Inner K_e ASME III

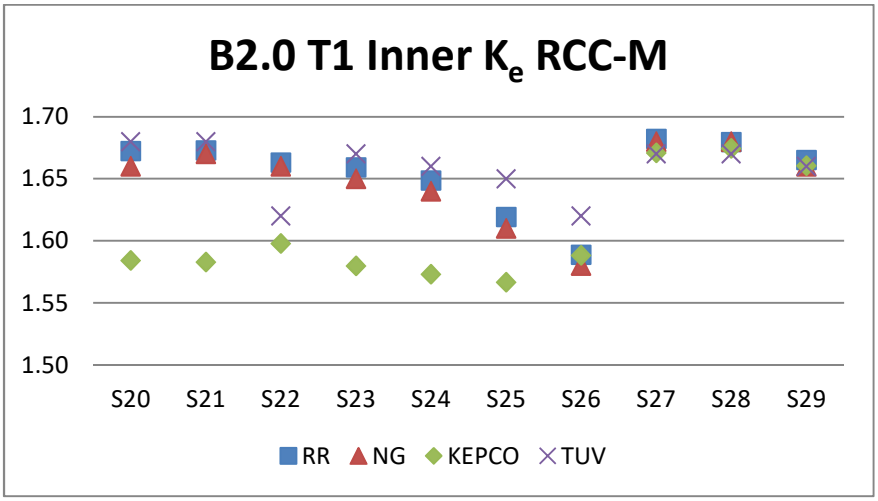

Figure 19. Benchmark 2.0 T1 inner K_e RCC-M

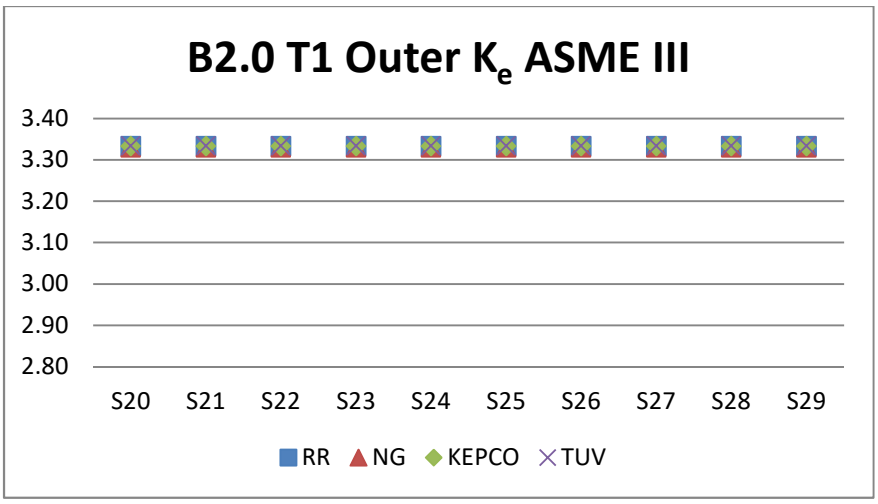

Figure 20. Benchmark 2.0 T1 outer K_e ASME III

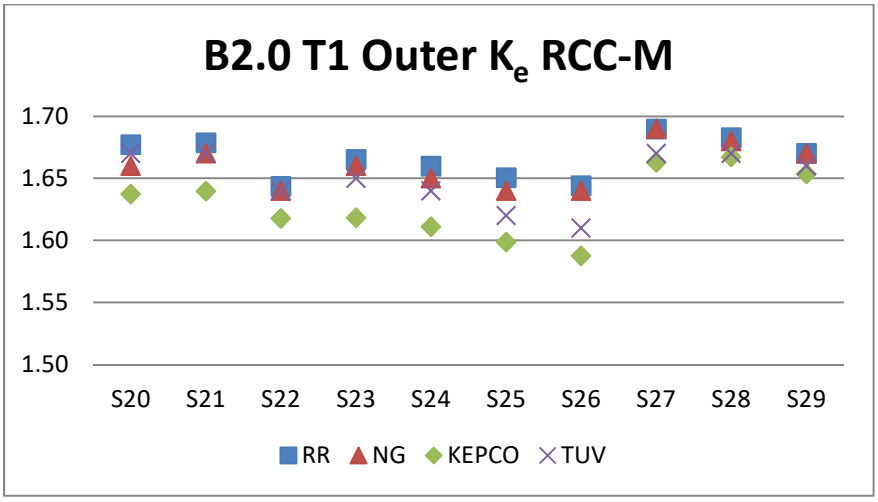

Figure 21. Benchmark 2.0 T1 outer K_e RCC-M

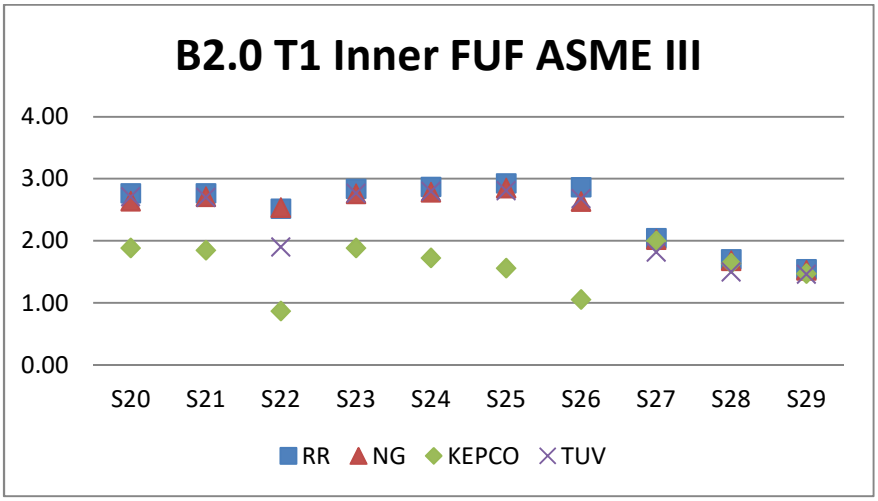

Figure 22. Benchmark 2.0 T1 inner FUF ASME III

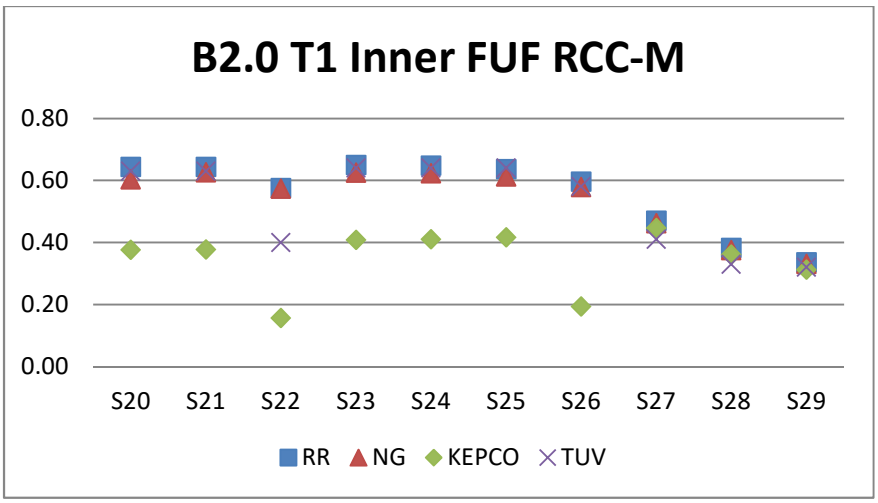

Figure 23. Benchmark 2.0 T1 inner FUF RCC-M

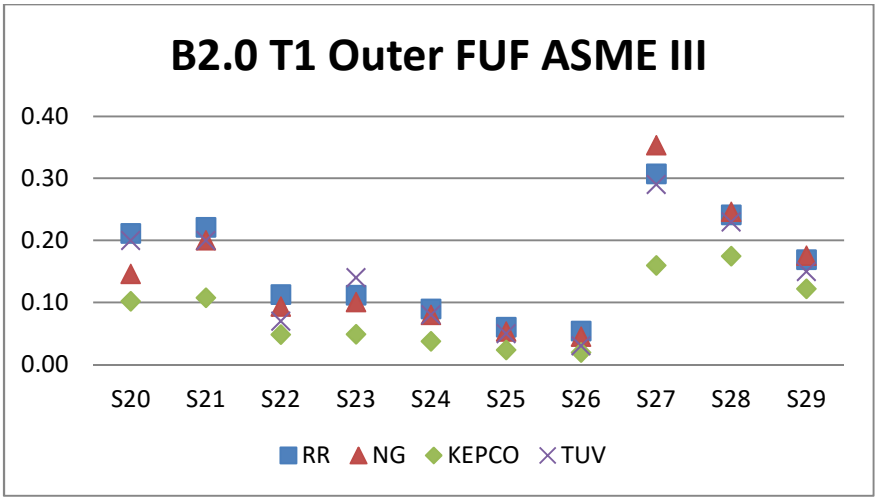

Figure 24. Benchmark 2.0 T1 outer FUF ASME III

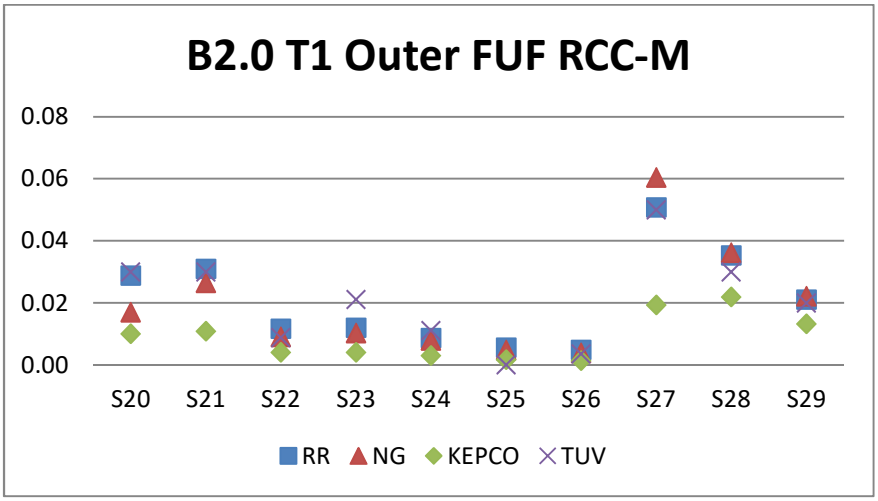

Figure 25. Benchmark 2.0 T1 outer FUF RCC-M

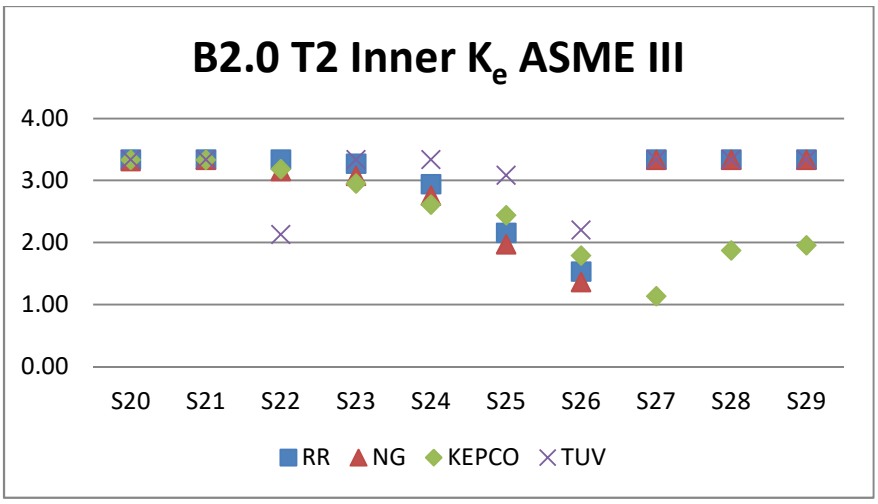

Figure 26. Benchmark 2.0 T2 inner K_e ASME III

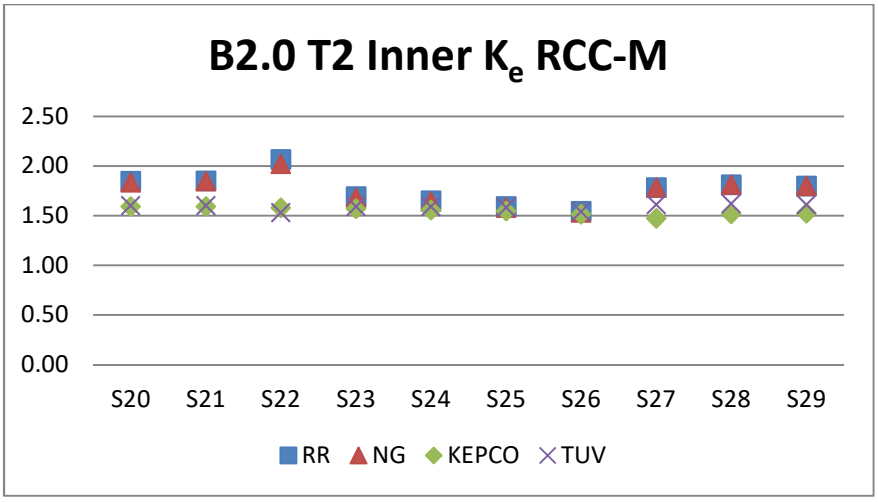

Figure 27. Benchmark 2.0 T2 inner K_e RCC-M

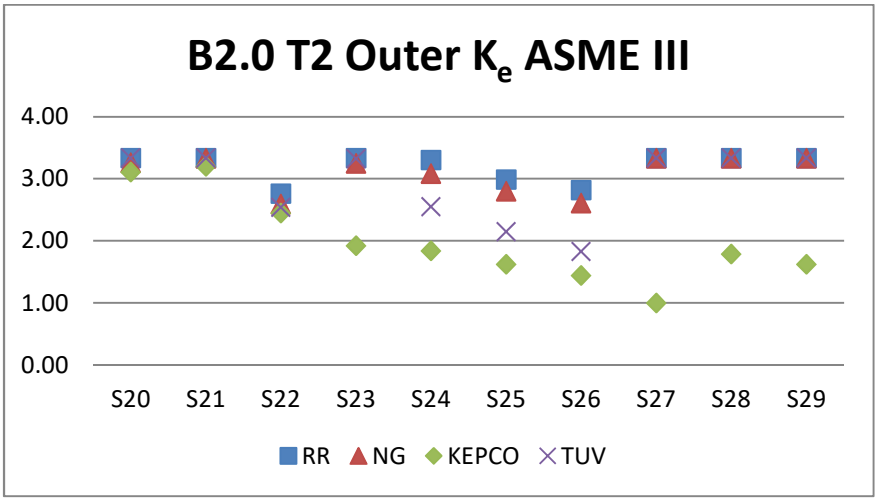

Figure 28. Benchmark 2.0 T2 outer K_e ASME III

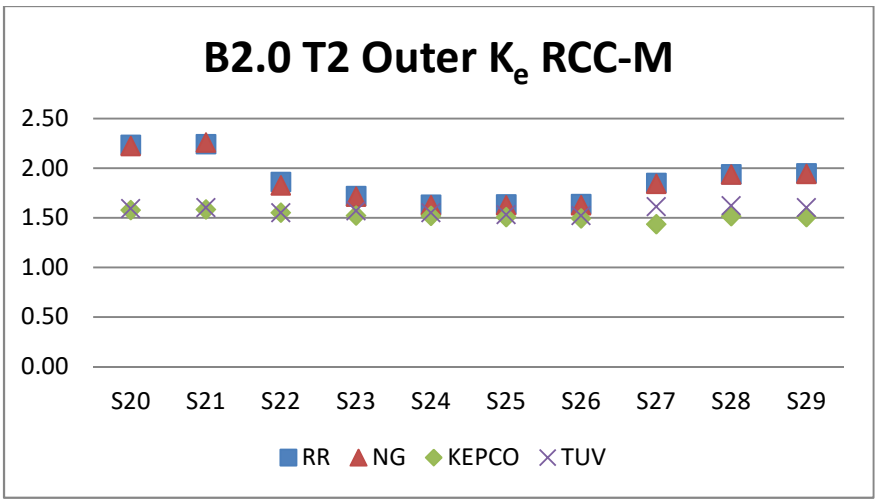

Figure 29. Benchmark 2.0 T2 outer K_e RCC-M

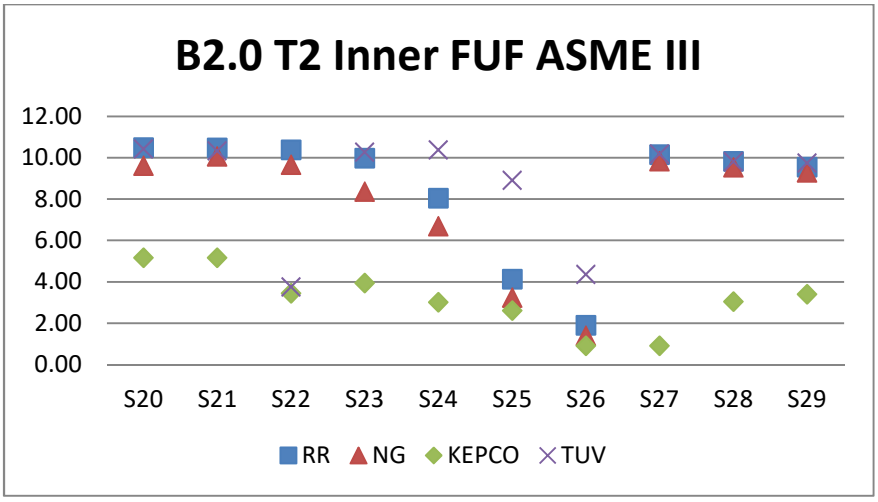

Figure 30. Benchmark 2.0 T2 inner FUF ASME III

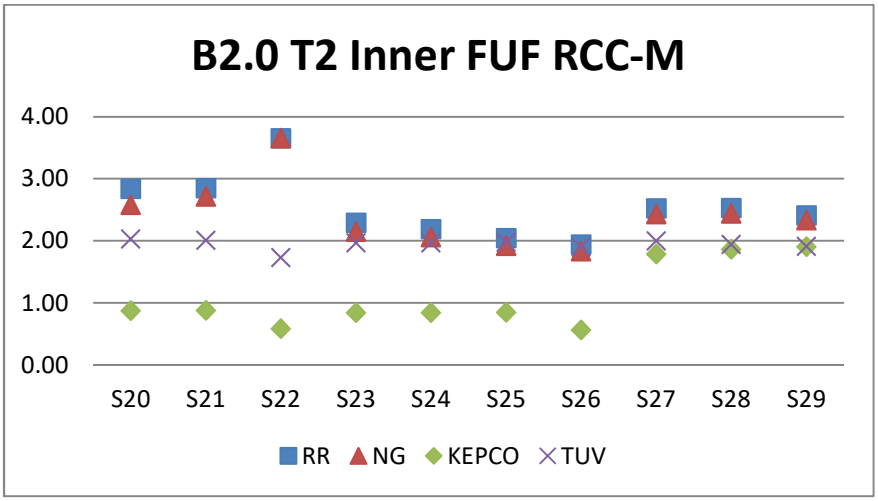

Figure 31. Benchmark 2.0 T2 inner FUF RCC-M

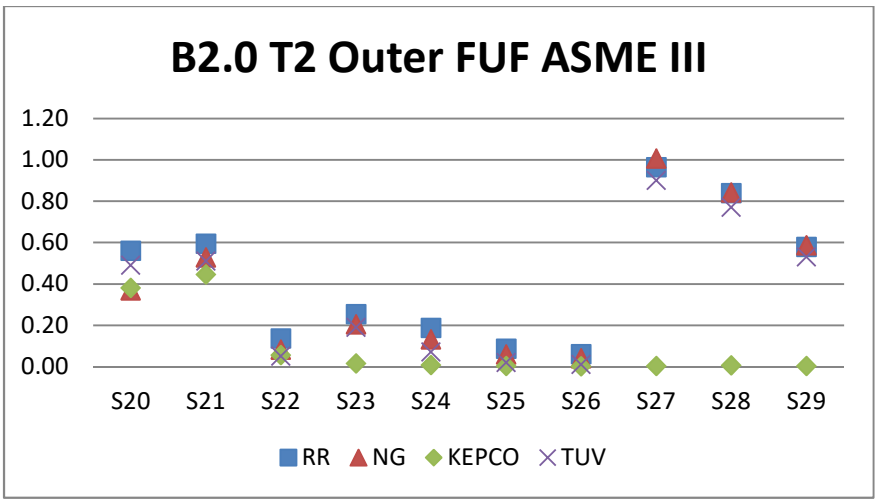

Figure 32. Benchmark 2.0 T2 outer FUF ASME III

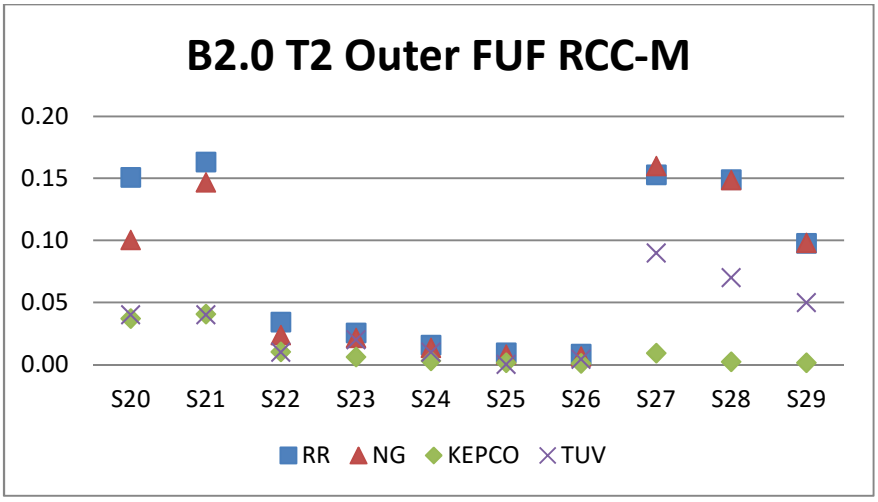

Figure 33. Benchmark 2.0 T2 outer FUF RCC-M

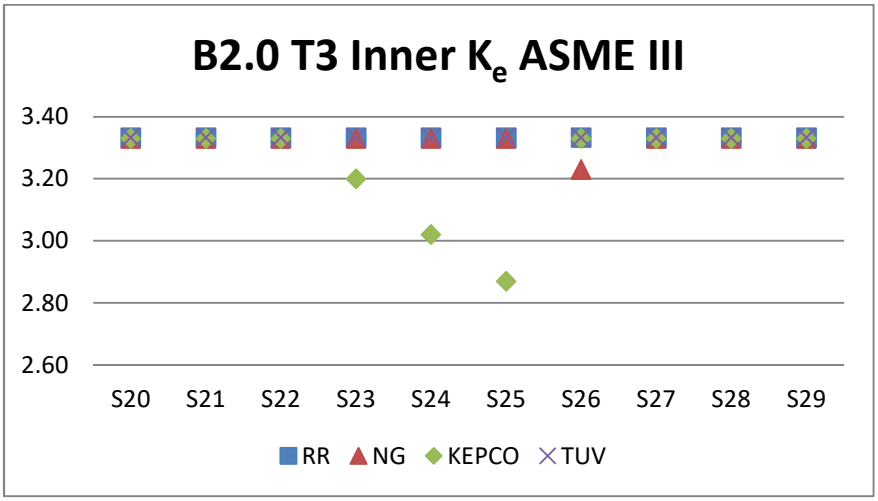

Figure 34. Benchmark 2.0 T3 inner K_e ASME III

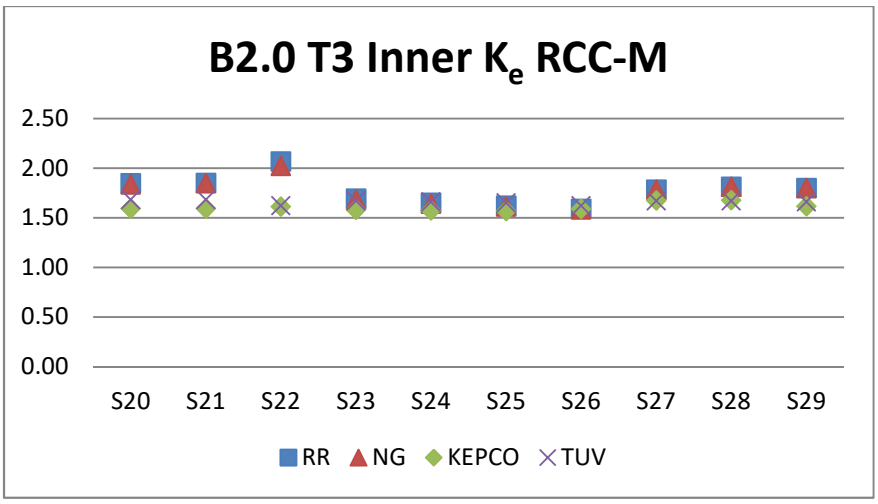

Figure 35. Benchmark 2.0 T3 inner K_e RCC-M

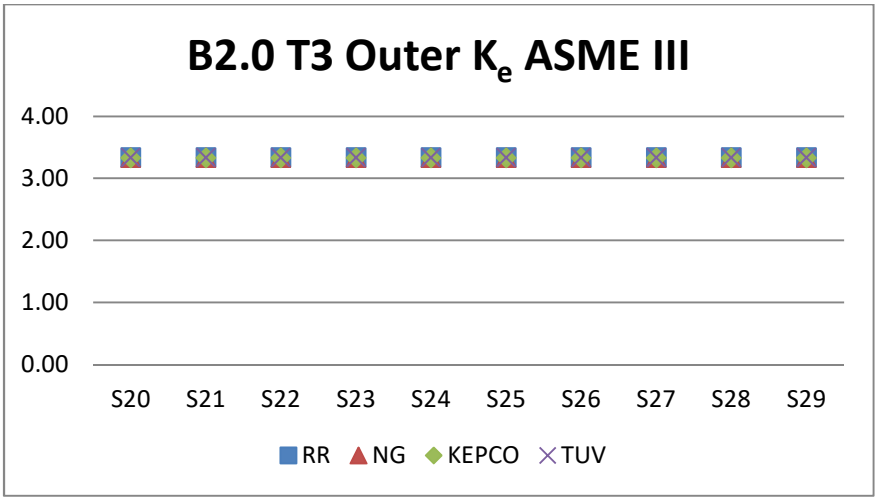

Figure 36. Benchmark 2.0 T3 outer K_e ASME III

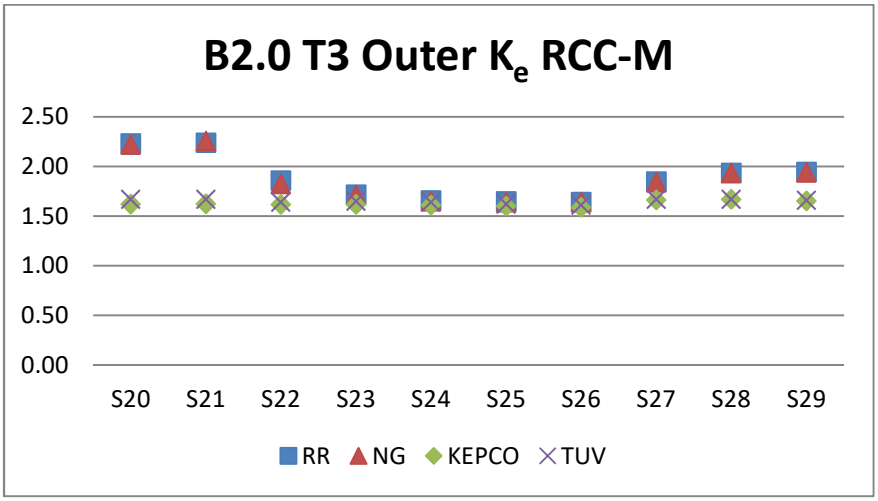

Figure 37. Benchmark 2.0 T3 outer K_e RCC-M

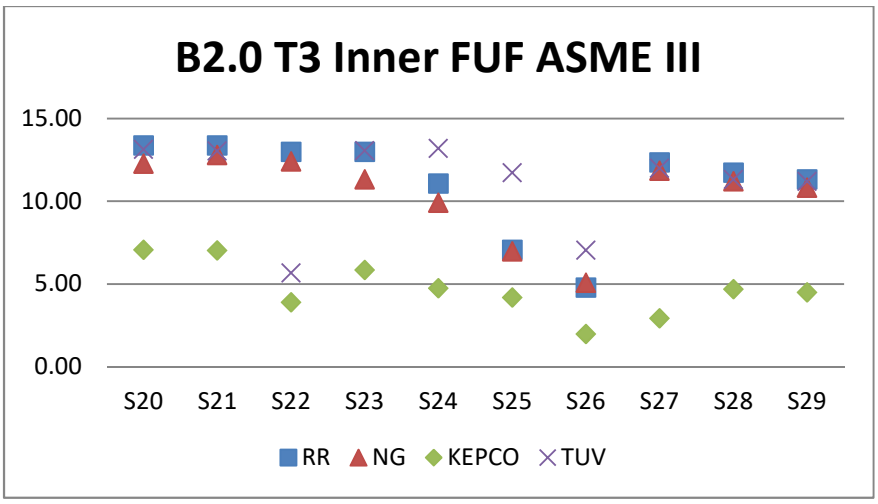

Figure 38. Benchmark 2.0 T3 inner FUF ASME III

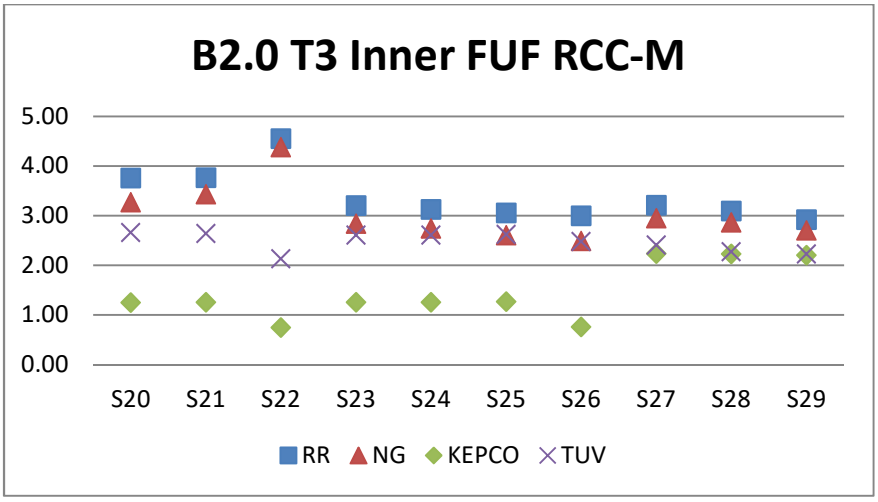

Figure 39. Benchmark 2.0 T3 inner FUF RCC-M

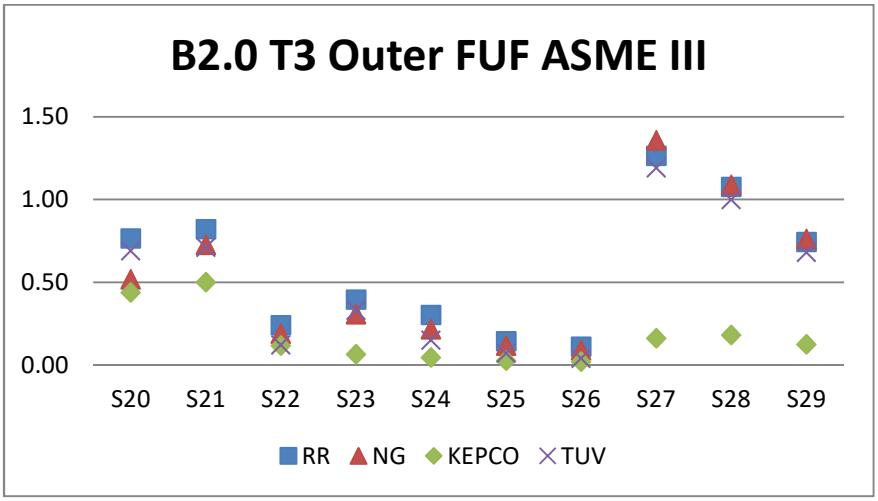

Figure 40. Benchmark 2.0 T3 outer FUF ASME III

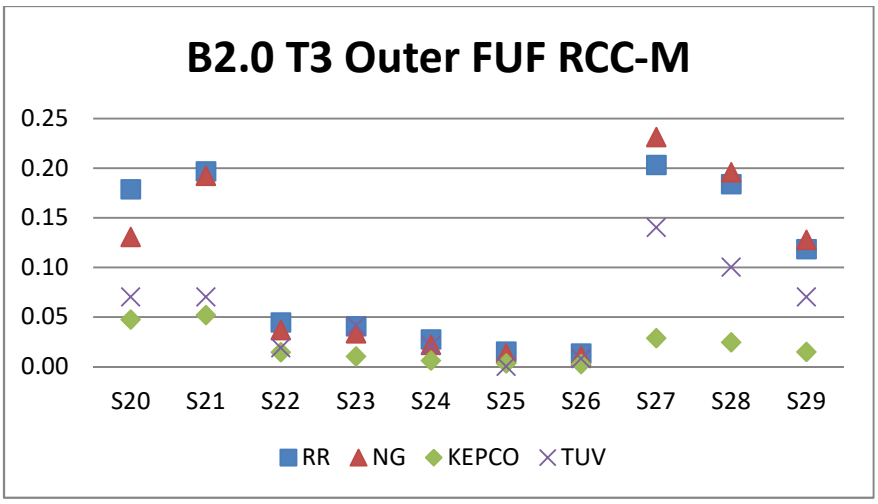

Figure 41. Benchmark 2.0 T3 outer FUF RCC-M

Table 8. Benchmark 2.0 – Total stress range (S_p) T1 & T2

	Assessment Location	Max. Total Stress Range (S_p)							
		Inner				Outer			
		Rolls-Royce	Naval Group	KEPCO-E&C	TUV	Rolls-Royce	Naval Group	KEPCO-E&C	TUV
Transient 1	S29	1287	1279	1251	1253	483	490	426	467
	S28	1348	1339	1318	1267	558	563	489	542
	S27	1471	1461	1446	1390	619	657	472	608
	S26	1733	1717	1710	1677	320	302	235	272
	S25	1752	1729	1722	1718	333	318	250	303
	S24	1735	1709	1703	1715	380	366	286	371
	S23	1726	1701	1694	1705	411	395	310	445
	S22	1628	1633	1577	1420	413	385	309	346
	S21	1704	1688	1673	1684	538	515	406	518
	S20	1705	1665	1673	1687	528	456	397	512
	Assessment Location	Max. Total Stress Range (S_p)							
		Inner				Outer			
		Rolls-Royce	Naval Group	KEPCO-E&C	TUV	Rolls-Royce	Naval Group	KEPCO-E&C	TUV
Transient 2	S29	1137.88	1123	1215	1149	353	355	162	343
	S28	1153.3	1137	1208	1153	402	402	177	389
	S27	1171.61	1154	1225	1173	424	431	250	413
	S26	1209.45	1192	1219	1201	213	201	159	200
	S25	1197.82	1177	1196	1192	221	212	169	205
	S24	1190.48	1168	1184	1185	253	243	191	248
	S23	1184.55	1161	1186	1179	273	262	213	251
	S22	1184.43	1210	1287	1160	273	252	238	224
	S21	1189.72	1167	1242	1182	357	343	337	339
	S20	1190.18	1149	1241	1187	350	309	329	334

Table 9. Benchmark 2.0 – Primary-plus-secondary stress range (S_n) T1 &T2

	Assessment Location	Max. Primary-Plus-Secondary Stress Range (S_n)							
		Inner				Outer			
		Rolls-Royce	Naval Group	KEPCO-E&C	TUV	Rolls-Royce	Naval Group	KEPCO-E&C	TUV
Transient 1	S29	805	798	782	803	830	819	750	763
	S28	883	872	854	829	901	886	816	836
	S27	897	891	834	856	945	934	794	840
	S26	530	511	529	627	709	683	527	578
	S25	619	599	635	754	737	713	558	626
	S24	729	707	672	798	779	754	593	683
	S23	776	752	708	820	804	778	616	726
	S22	795	764	545	627	707	685	637	681
	S21	844	819	703	858	877	850	692	836
	S20	843	792	705	861	868	787	683	831
	Assessment Location	Max. Primary-Plus-Secondary Stress Range (S_n)							
		Inner				Outer			
		Rolls-Royce	Naval Group	KEPCO-E&C	TUV	Rolls-Royce	Naval Group	KEPCO-E&C	TUV
Transient 2	S29	593	582	393	594	611	597	363	565
	S28	641	628	386	609	654	637	379	609
	S27	619	611	332	594	654	642	306	580
	S26	355	339	378	416	474	454	347	382
	S25	412	395	438	497	489	471	363	412
	S24	484	467	453	524	516	497	383	448
	S23	514	496	485	538	532	512	395	479
	S22	526	504	506	410	468	452	439	447
	S21	560	541	538	564	582	561	512	549
	S20	559	518	540	566	576	513	504	546

Table 10. Benchmark 2.0 – Ke ASME III T1 & T2

	Assessment Location	ASME III Plasticity Correction Factor (K_e)							
		Inner				Outer			
		Rolls-Royce	Naval Group	KEPCO-E&C	TUV	Rolls-Royce	Naval Group	KEPCO-E&C	TUV
Transient 1	S29	3.33	3.33	3.33	3.33	3.33	3.33	3.33	3.33
	S28	3.33	3.33	3.33	3.33	3.33	3.33	3.33	3.33
	S27	3.33	3.33	3.33	3.33	3.33	3.33	3.33	3.33
	S26	3.33	3.23	3.33	3.33	3.33	3.33	3.33	3.33
	S25	3.33	3.33	2.87	3.33	3.33	3.33	3.33	3.33
	S24	3.33	3.33	3.02	3.33	3.33	3.33	3.33	3.33
	S23	3.33	3.33	3.20	3.33	3.33	3.33	3.33	3.33
	S22	3.33	3.33	3.33	3.33	3.33	3.33	3.33	3.33
	S21	3.33	3.33	3.28	3.33	3.33	3.33	3.33	3.33
	S20	3.33	3.33	3.32	3.33	3.33	3.33	3.33	3.33
	Assessment Location	ASME III Plasticity Correction Factor (K_e)							
		Inner				Outer			
		Rolls-Royce	Naval Group	KEPCO-E&C	TUV	Rolls-Royce	Naval Group	KEPCO-E&C	TUV
Transient 2	S29	3.33	3.33	1.95	3.33	3.33	3.33	1.62	3.33
	S28	3.33	3.33	1.87	3.33	3.33	3.33	1.79	3.33
	S27	3.33	3.33	1.13	3.33	3.33	3.33	1.00	3.33
	S26	1.53	1.36	1.79	2.20	2.82	2.61	1.44	1.83
	S25	2.15	1.97	2.44	3.08	2.99	2.8	1.62	2.15
	S24	2.94	2.75	2.61	3.33	3.31	3.08	1.84	2.55
	S23	3.27	3.07	2.95	3.33	3.33	3.25	1.92	3.33
	S22	3.33	3.15	3.18	2.13	2.76	2.59	2.45	2.54
	S21	3.33	3.33	3.33	3.33	3.33	3.33	3.20	3.33
	S20	3.33	3.31	3.33	3.33	3.33	3.26	3.11	3.33

Table 11. Benchmark 2.0 – K_e RCC-M T1 & T2

	Assessment Location	RCC-M Plasticity Correction Factor (K_e)							
		Inner				Outer			
		Rolls-Royce	Naval Group	KEPCO-E&C	TUV	Rolls-Royce	Naval Group	KEPCO-E&C	TUV
Transient 1	S29	1.67	1.66	1.66	1.66	1.67	1.67	1.65	1.66
	S28	1.68	1.68	1.67	1.67	1.68	1.68	1.67	1.67
	S27	1.68	1.68	1.67	1.67	1.69	1.69	1.66	1.67
	S26	1.59	1.58	1.59	1.62	1.64	1.64	1.59	1.61
	S25	1.62	1.61	1.57	1.65	1.65	1.64	1.60	1.62
	S24	1.65	1.64	1.57	1.66	1.66	1.65	1.61	1.64
	S23	1.66	1.65	1.58	1.67	1.67	1.66	1.62	1.65
	S22	1.66	1.66	1.60	1.62	1.64	1.64	1.62	1.64
	S21	1.67	1.67	1.58	1.68	1.68	1.67	1.64	1.67
	S20	1.67	1.66	1.58	1.68	1.68	1.66	1.64	1.67
	Assessment Location	RCC-M Plasticity Correction Factor (K_e)							
		Inner				Outer			
		Rolls-Royce	Naval Group	KEPCO-E&C	TUV	Rolls-Royce	Naval Group	KEPCO-E&C	TUV
Transient 2	S29	1.80	1.80	1.52	1.61	1.95	1.94	1.50	1.60
	S28	1.81	1.81	1.52	1.62	1.94	1.93	1.51	1.62
	S27	1.78	1.78	1.47	1.61	1.85	1.84	1.43	1.61
	S26	1.54	1.53	1.51	1.54	1.64	1.62	1.49	1.52
	S25	1.59	1.58	1.55	1.58	1.63	1.62	1.50	1.53
	S24	1.65	1.64	1.56	1.59	1.63	1.62	1.52	1.55
	S23	1.69	1.68	1.57	1.59	1.72	1.71	1.52	1.57
	S22	2.06	2.02	1.58	1.53	1.86	1.82	1.55	1.55
	S21	1.85	1.85	1.59	1.60	2.24	2.26	1.58	1.60
	S20	1.84	1.83	1.59	1.60	2.23	2.22	1.58	1.59

Table 12. Benchmark 2.0 – FUF ASME III T1 & T2

	Assessment Location	ASME III Fatigue Usage Factor (FUF)							
		Inner				Outer			
		Rolls-Royce	Naval Group	KEPCO-E&C	TUV	Rolls-Royce	Naval Group	KEPCO-E&C	TUV
Transient 1	S29	1.55	1.53	1.47	1.46	0.17	0.18	0.12	0.15
	S28	1.70	1.68	1.64	1.50	0.24	0.25	0.17	0.23
	S27	2.05	2.02	2.00	1.82	0.31	0.35	0.16	0.29
	S26	2.86	2.63	1.05	2.68	0.05	0.04	0.02	0.03
	S25	2.93	2.85	1.56	2.81	0.06	0.05	0.02	0.05
	S24	2.87	2.78	1.72	2.80	0.09	0.08	0.04	0.08
	S23	2.84	2.76	1.89	2.77	0.11	0.10	0.05	0.14
	S22	2.52	2.54	0.87	1.90	0.11	0.09	0.05	0.07
	S21	2.77	2.71	1.85	2.70	0.22	0.20	0.11	0.20
	S20	2.77	2.64	1.89	2.71	0.21	0.15	0.10	0.20
	Assessment Location	ASME III Fatigue Usage Factor (FUF)							
		Inner				Outer			
		Rolls-Royce	Naval Group	KEPCO-E&C	TUV	Rolls-Royce	Naval Group	KEPCO-E&C	TUV
Transient 2	S29	9.54	9.28	3.40	9.74	0.58	0.59	0.002	0.53
	S28	9.81	9.52	3.04	9.81	0.84	0.84	0.005	0.77
	S27	10.14	9.82	0.91	10.17	0.96	1.01	0.002	0.9
	S26	1.90	1.39	0.91	4.36	0.06	0.04	0.001	0.01
	S25	4.13	3.23	2.61	8.9	0.09	0.06	0.002	0.02
	S24	8.04	6.68	3.01	10.38	0.19	0.13	0.007	0.07
	S23	9.97	8.35	3.94	10.27	0.25	0.20	0.015	0.19
	S22	10.38	9.66	3.45	3.75	0.14	0.08	0.056	0.05
	S21	10.48	10.06	5.16	10.33	0.59	0.53	0.444	0.51
	S20	10.49	9.60	5.16	10.42	0.56	0.37	0.380	0.49

Table 13. Benchmark 2.0 – FUF RCC-M T1 & T2

	Assessment Location	RCC-M Fatigue Usage Factor (FUF)							
		Inner				Outer			
		Rolls-Royce	Naval Group	KEPCO-E&C	TUV	Rolls-Royce	Naval Group	KEPCO-E&C	TUV
Transient 1	S29	0.34	0.33	0.31	0.32	0.02	0.02	0.013	0.020
	S28	0.38	0.37	0.36	0.33	0.04	0.04	0.022	0.030
	S27	0.47	0.46	0.45	0.41	0.05	0.06	0.019	0.050
	S26	0.60	0.58	0.19	0.58	0.00	0.00	0.001	0.004
	S25	0.64	0.61	0.42	0.64	0.01	0.00	0.002	0.000
	S24	0.65	0.62	0.41	0.64	0.01	0.01	0.003	0.011
	S23	0.65	0.63	0.41	0.64	0.01	0.01	0.004	0.021
	S22	0.57	0.57	0.16	0.40	0.01	0.01	0.004	0.009
	S21	0.64	0.63	0.38	0.63	0.03	0.03	0.011	0.030
	S20	0.64	0.60	0.38	0.63	0.03	0.02	0.010	0.030
	Assessment Location	RCC-M Fatigue Usage Factor (FUF)							
		Inner				Outer			
		Rolls-Royce	Naval Group	KEPCO-E&C	TUV	Rolls-Royce	Naval Group	KEPCO-E&C	TUV
Transient 2	S29	2.41	2.33	1.90	1.91	0.10	0.10	0.001	0.050
	S28	2.53	2.44	1.86	1.94	0.15	0.15	0.002	0.070
	S27	2.52	2.43	1.79	2.00	0.15	0.16	0.009	0.090
	S26	1.94	1.84	0.57	1.90	0.01	0.01	0.001	0.004
	S25	2.04	1.92	0.85	1.98	0.01	0.01	0.001	0.000
	S24	2.19	2.06	0.84	1.97	0.02	0.01	0.003	0.010
	S23	2.29	2.15	0.84	1.97	0.03	0.02	0.006	0.020
	S22	3.65	3.66	0.58	1.73	0.03	0.02	0.010	0.010
	S21	2.85	2.72	0.88	2.01	0.16	0.15	0.041	0.040
	S20	2.84	2.58	0.87	2.03	0.15	0.10	0.037	0.040

Table 14. Benchmark 2.0 – FUF ASME III & RCC-M T3

	Assessment Location	ASME III Fatigue Usage Factor (FUF)							
		Inner				Outer			
		Rolls-Royce	Naval Group	KEPCO-E&C	TUV	Rolls-Royce	Naval Group	KEPCO-E&C	TUV
Transient 1+2 (T3)	S29	11.31	10.80	4.47	11.20	0.76	0.74	0.124	0.680
	S28	11.72	11.20	4.68	11.31	1.09	1.08	0.180	1.000
	S27	12.34	11.84	2.91	11.99	1.36	1.26	0.161	1.190
	S26	4.77	5.06	1.96	7.04	0.09	0.11	0.020	0.040
	S25	7.05	6.95	4.18	11.71	0.12	0.14	0.026	0.070
	S24	11.06	9.89	4.73	13.18	0.22	0.30	0.045	0.150
	S23	12.97	11.31	5.83	13.04	0.31	0.40	0.064	0.330
	S22	12.97	12.40	3.89	5.65	0.19	0.24	0.117	0.120
	S21	13.36	12.77	7.01	13.03	0.73	0.82	0.501	0.710
	S20	13.36	12.26	7.05	13.13	0.52	0.77	0.438	0.690
	Assessment Location	RCC-M Fatigue Usage Factor (FUF)							
		Inner				Outer			
		Rolls-Royce	Naval Group	KEPCO-E&C	TUV	Rolls-Royce	Naval Group	KEPCO-E&C	TUV
Transient 1+2 (T3)	S29	2.92	2.70	2.20	2.23	0.12	0.13	0.015	0.070
	S28	3.09	2.86	2.23	2.27	0.18	0.20	0.024	0.100
	S27	3.21	2.94	2.24	2.41	0.20	0.23	0.028	0.140
	S26	2.99	2.49	0.76	2.48	0.01	0.01	0.002	0.008
	S25	3.05	2.60	1.27	2.62	0.01	0.01	0.003	0.000
	S24	3.13	2.74	1.25	2.61	0.03	0.02	0.006	0.021
	S23	3.20	2.83	1.25	2.61	0.04	0.03	0.010	0.041
	S22	4.55	4.37	0.75	2.13	0.04	0.04	0.014	0.019
	S21	3.77	3.43	1.26	2.64	0.20	0.19	0.052	0.070
	S20	3.75	3.27	1.25	2.66	0.18	0.13	0.047	0.070

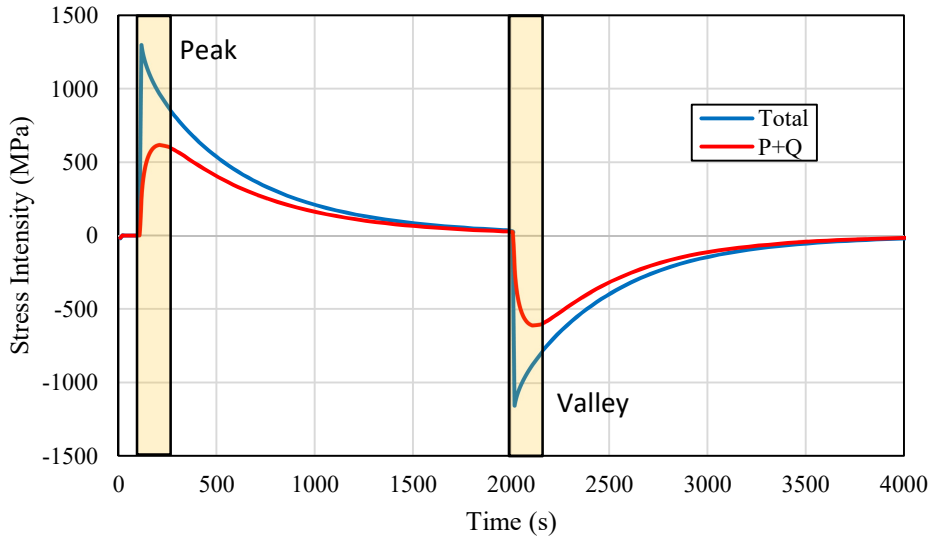

Figure 42. Illustration of peak-valley search within time window

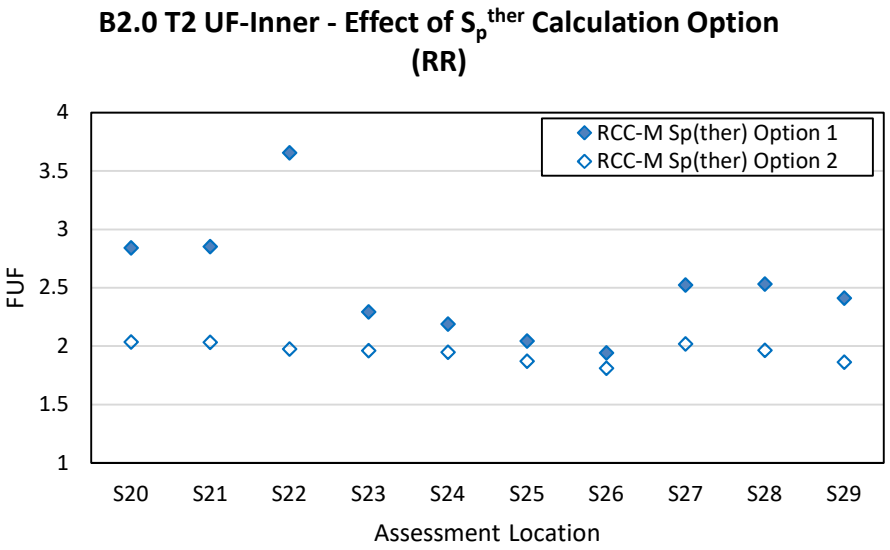

Figure 43. Effect of S_p^{ther} calculation on T2 inner FUF RCC-M

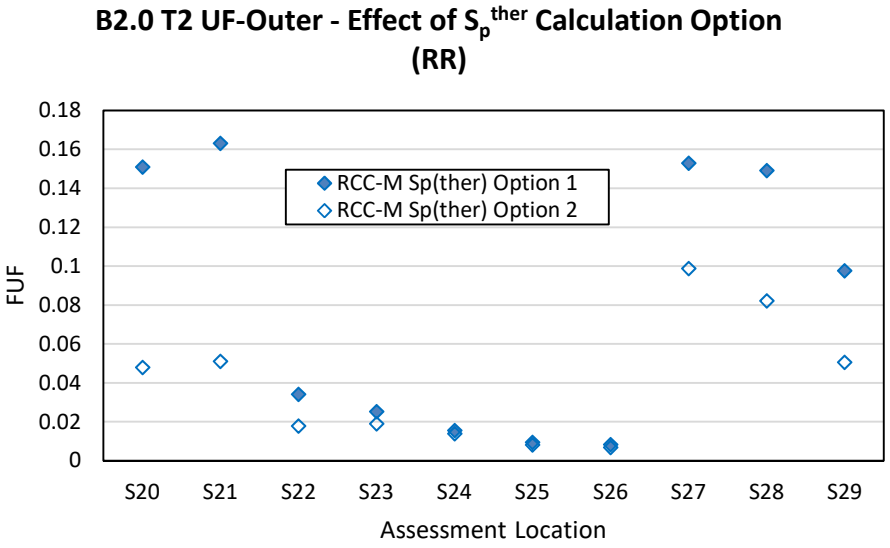

Figure 44. Effect of S_p^{ther} calculation on T2 Outer FUF RCC-M

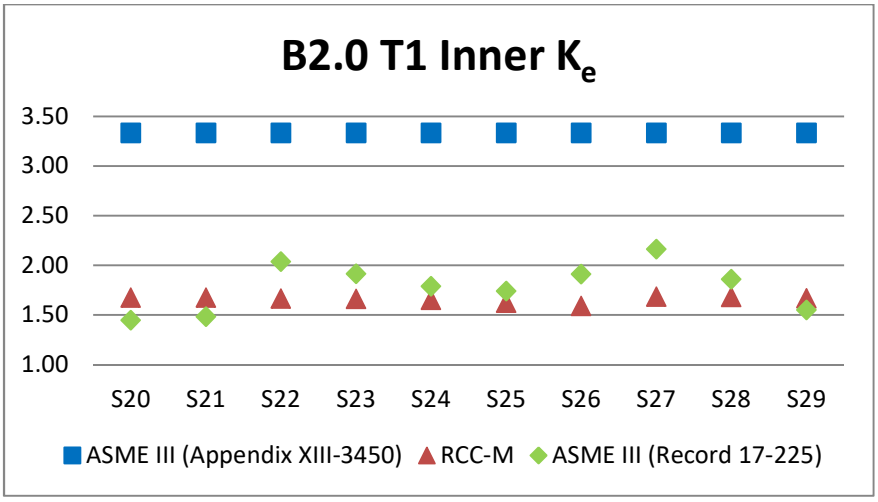

Figure 45. Benchmark 2.0 T1 inner code K_e comparison

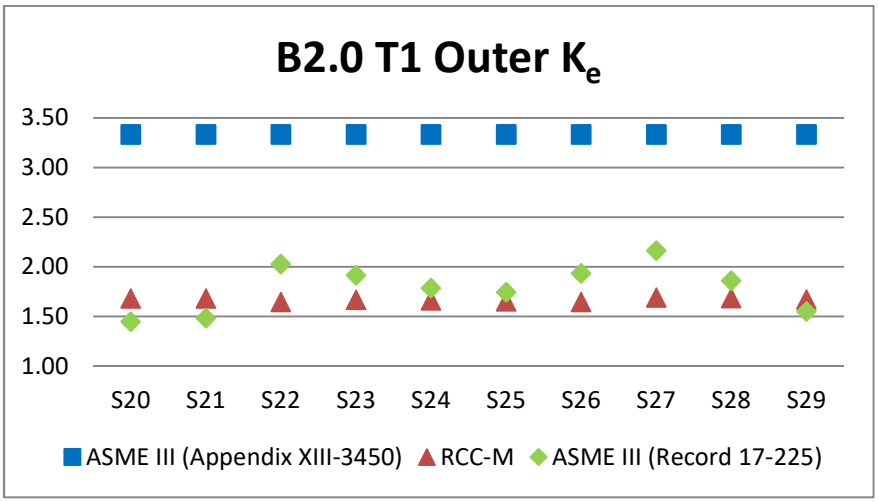

Figure 46. Benchmark 2.0 T1 outer code K_e comparison

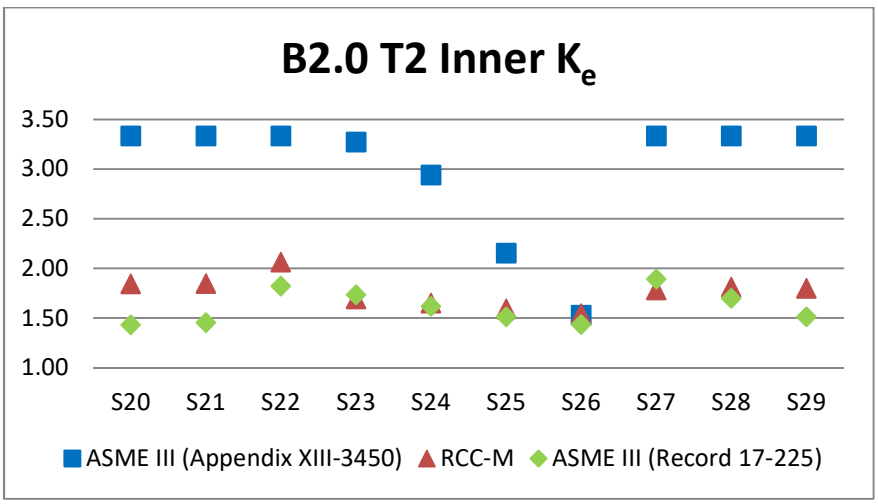

Figure 47. Benchmark 2.0 T2 inner code K_e comparison

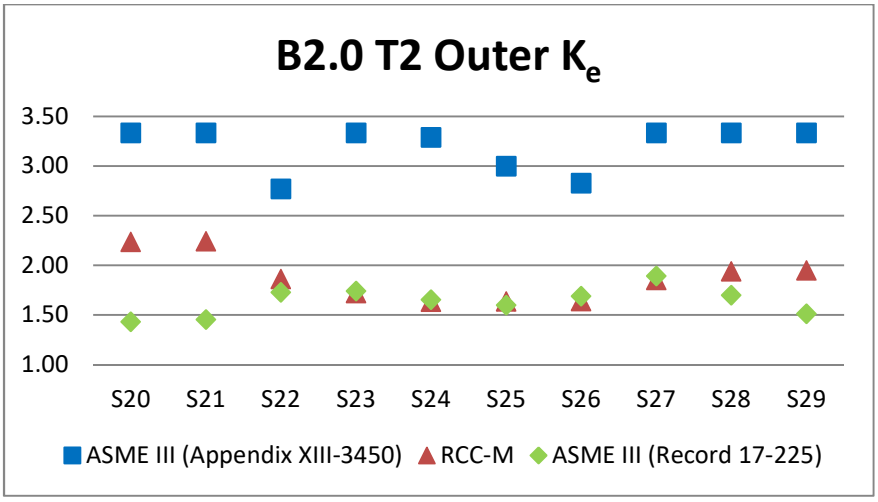

Figure 48. Benchmark 2.0 T2 outer code K_e comparison

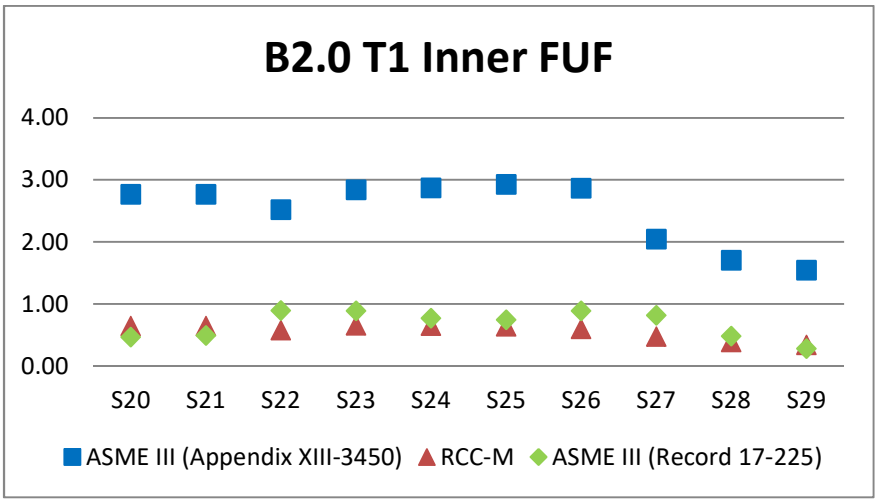

Figure 49. Benchmark 2.0 T1 inner code FUF comparison

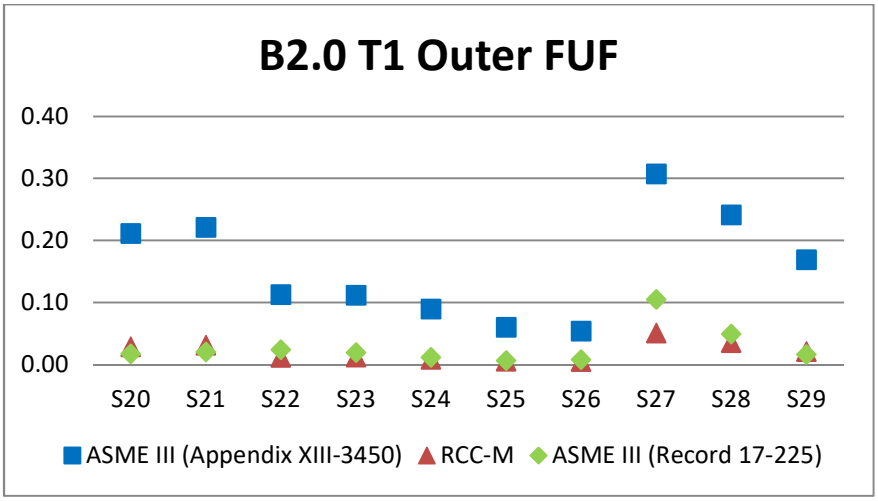

Figure 50. Benchmark 2.0 T1 outer code FUF comparison

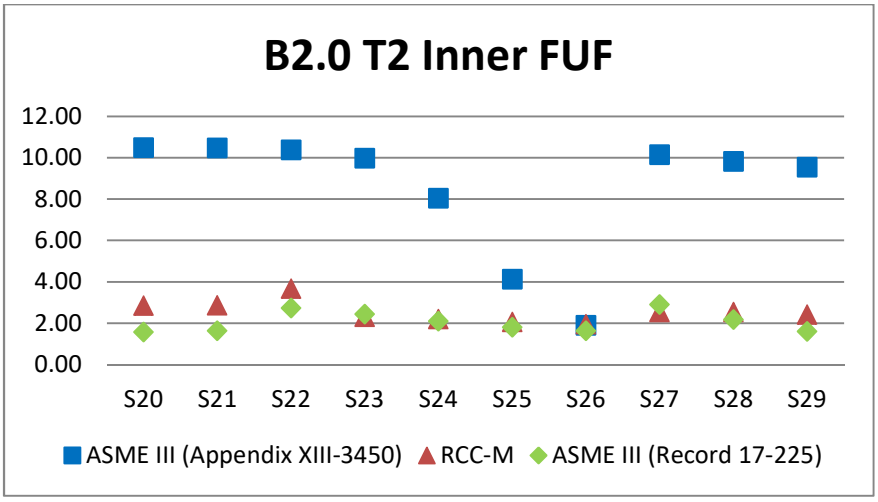

Figure 51. Benchmark 2.0 T2 inner code FUF comparison

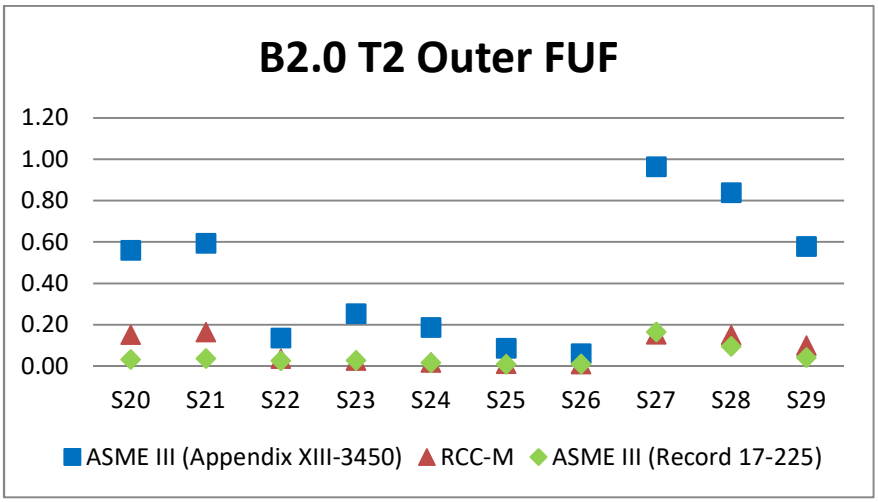

Figure 52. Benchmark 2.0 T2 outer code FUF comparison

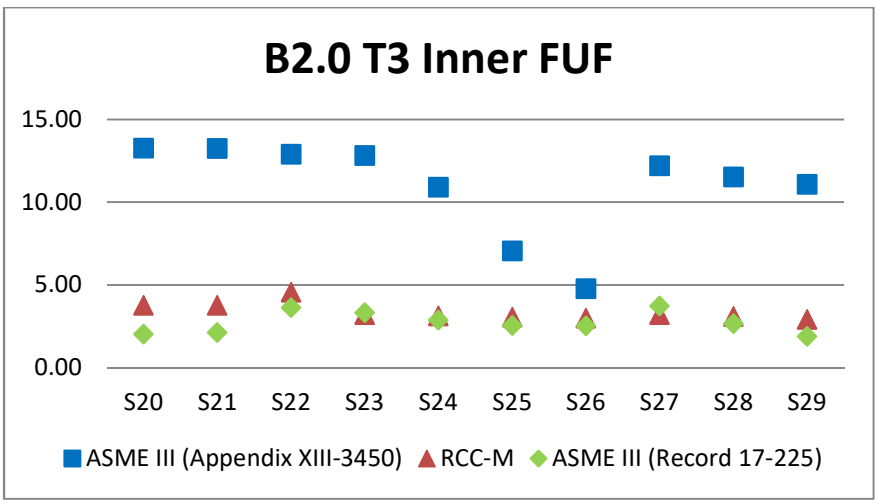

Figure 53. Benchmark 2.0 T3 inner code FUF comparison

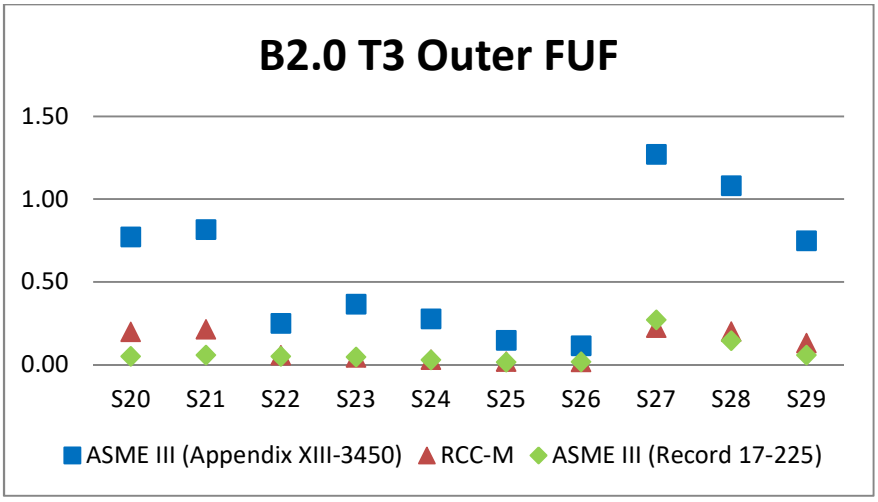

Figure 54. Benchmark 2.0 T3 outer code FUF comparison

3.2 Benchmark 2.1: MCL Nozzle – Fatigue simplified non-linear analyses

The purpose of Benchmark 2.1 is to examine the use of simplified methods of elastic-plastic FEA to take account of plasticity in evaluating fatigue life. K_e is obtained directly from the ratio of the elastic-plastic strain range calculated by elastic-plastic FEA to the elastic strain range determined from an equivalent elastic analysis. Two quantities, the FE-derived plasticity correction factor, K_e, and the FUF are obtained for the inner and outer surfaces of sections S20 to S29 considering the three transients T1, T2 and T1+T2 (T3). The Type 316L stress-strain curve defined in Appendix A4.2 of reference [2] is to be utilized for this problem.

The Benchmark 2.1 calculation is a theoretical exercise and does not represent the true cyclic stress-strain response of structures, as the isotropic model is not able to take into account the Bauschinger effect, and therefore is not valid for cyclic complex loads. The purpose of this analysis is only to compare participants' results with a first easy step of non-linear assessment of fatigue before taking into account more complex constitutive cyclic models in Benchmark 2.3. Due to the nature of unlimited isotropic hardening, strict shakedown is established immediately following the first loading cycle. It is therefore only necessary to simulate a single full cycle of the design transients for the purposes of this benchmark problem. The elastic-plastic equivalent strain range is calculated according to the von Mises criterion, consistent with the method described in Section 4.7 of reference [2].

Three participants have submitted results for Benchmark 2.1. Figures 55 to 66 summarize the K_e and FUF results obtained by each participant. Detailed tabulated results showing the elastic-plastic strain range, FE-derived K_e factors, and FUFs are provided in Tables 15, 16 and 17, respectively. Note that where the elastic-plastic strain range was not provided by the participant, it was reverse-engineered from the reported FUF; in some cases this was however not possible (e.g. where the FUF was so low as to be counted as zero by the participant) and therefore these tabulated values are marked as 'N/A'. A general examination of the results reveals that the K_e factors calculated in this way are significantly less than the code K_e factors. Whilst some differences in the calculated K_e and FUF values were observed between participants, the general trend was found to be similar overall. Some reasons for these differences are proposed later.

The K_e factors calculated for this problem are shown in Figures 55 to 60. Participants agreed that for Transient 1, the maximum K_e occurs in the nozzle region (S23-S26) and is lowest at the nozzle crotch corner (S22). On the other hand, for Transient 2, there was a difference of agreement in the location of the maximum K_e, where two participants (RR and TUV) determined K_e to be highest in the branch pipe (S27-S29), whilst another participant (NG) determined K_e to be highest in the nozzle (S25). The reasons for this difference were unclear, but possible reasons may be due to difference in the stress adopted to define the onset of plasticity in the FE software (i.e. the cyclic yield strength, S_y^c). Due to the definition of Transient 2, it is however expected that the majority of the inner surface should experience a relatively similar level of plastic straining. The reasoning for this is that due to the sharp nature of the thermal shock, the thermal gradient developed across both thin and thick sections will initially be very similar, thereby inducing similar surface strains irrespective of section thickness.

It is also important to remember that the K_e factor is not related to strain intensity itself, but is simply the ratio of the strains determined respectively by elastic-plastic and elastic analysis. Thus, the location of maximum K_e does not necessarily correspond to the location of highest FUF. It should also be noted that for regions of low stress, usually on the outer surface where S_p remains less than $3S_m$, stress redistribution means that K_e must go below unity to maintain the overall balance of deformations within the component. This can be understood from the elastic follow-up concept, whereby the elastic recovery or 'spring-back effect' of the region of higher rigidity (i.e. the elastic region within the wall thickness) enhances the displacement of the lower rigidity region (i.e. the internal surface which suffers loss of constraint), since the total displacement is constant and thus results in strain concentration on the inner surface. Some participants opted to report K_e values which were less than unity, whilst others instead adopted a default value of $K_e = 1.0$ for any $K_e < 1.0$.

The FUFs calculated for this problem are shown in Figures 61 to 66. Participants agreed that the highest FUFs considering both Transient 1 and 2 were situated in the nozzle region (S23-S26). This is largely due the higher thermal resistance of the nozzle, leading to higher surface strains. Participants also agreed that the location of highest FUF for the combination of Transient 1 and Transient 2 (T3) was at S25. However, it was also acknowledged that participants adopted different methods for calculating the K_e and FUF for the transient combination. Two participants (RR and TUV) calculated results for T3 based on an approach common to ASME III plastic analysis evaluations. In this approach, the elastic-plastic fatigue evaluation is performed for each fatigue cycle pair individually and the fatigue usage factors obtained by a summation. Since this problem considers only inside pairs, this amounted to performing a linear summation of the FUFs obtained from T1 and T2, without analysing T3 separately. On the other hand, NG adopted a different approach consistent with the RCC-M transient combination method, wherein an additional non-linear analysis was conducted to determine the FUF in common with 100 cycles of T1+T2, and the 700 remaining cycles of T2.

The participants also discussed the following points:

(i) Accuracy of stress-strain curve fit (bi-linear, multi-linear, etc.).

(ii) Choice of cyclic yield strength, S_y^c, adopted in FE analysis.

In this benchmark problem, all participants adopted a multi-linear fit of the cyclic stress-strain curve for simulation within FE software, and therefore the accuracy of the curve fit was not thought to be a significant factor in results differences.

A more important factor is the stress amplitude used to define the onset of plasticity behaviour in the FE software. One participant (RR) defined the onset of plasticity at S_y^c = $1.5S_m$ = 153 MPa to be consistent with $3S_m$ criterion of both ASME III and RCC-M. Another participant (NG) adopted S_y^c = S_y = 92 MPa, where S_y is specified in Appendix 4.1 of [2], to define the limit of the elastic domain. Other options could also be justified. Differences in the adopted value of S_y^c are believed to have a more significant effect on the K_e and FUF results as it directly influences the magnitude of plastic strains computed in the FE software.

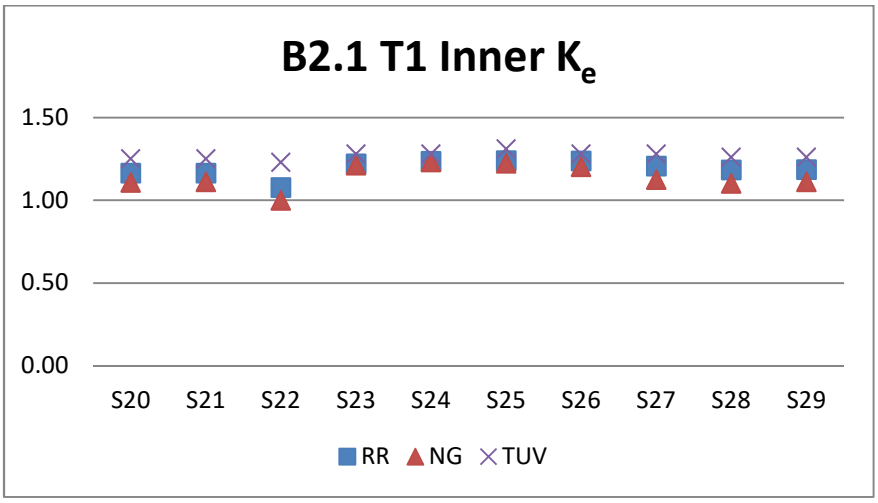

Figure 55. Benchmark 2.1 T1 inner K_e

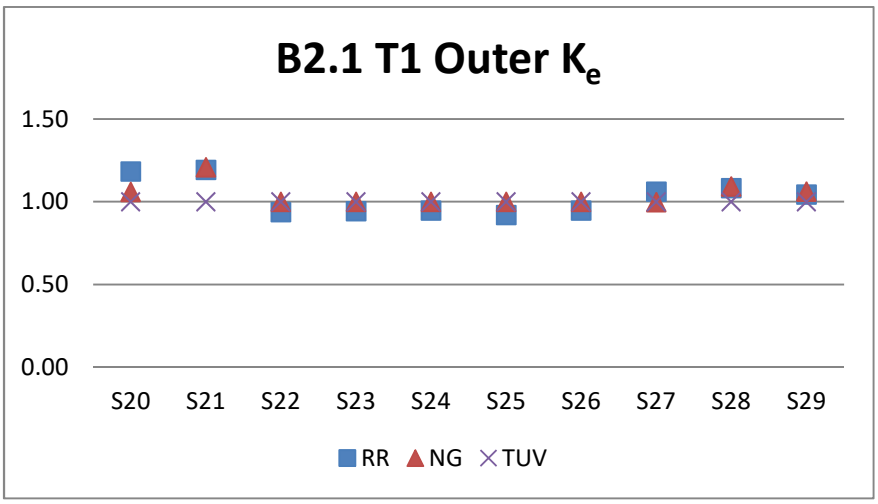

Figure 56. Benchmark 2.1 T1 outer K_e

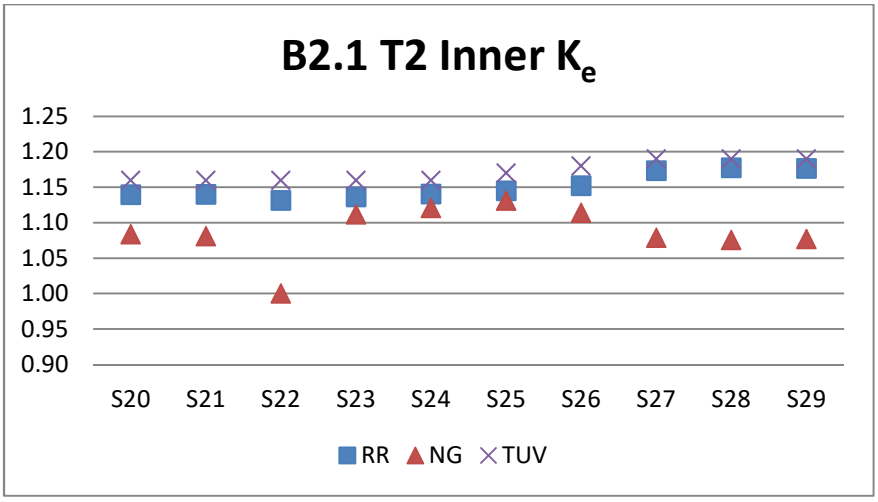

Figure 57. Benchmark 2.1 T2 inner K_e

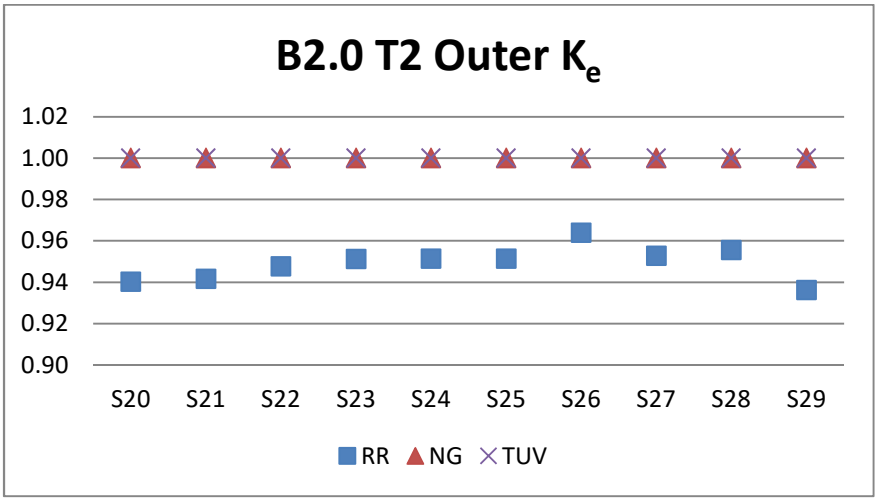

Figure 58. Benchmark 2.1 T2 outer K_e

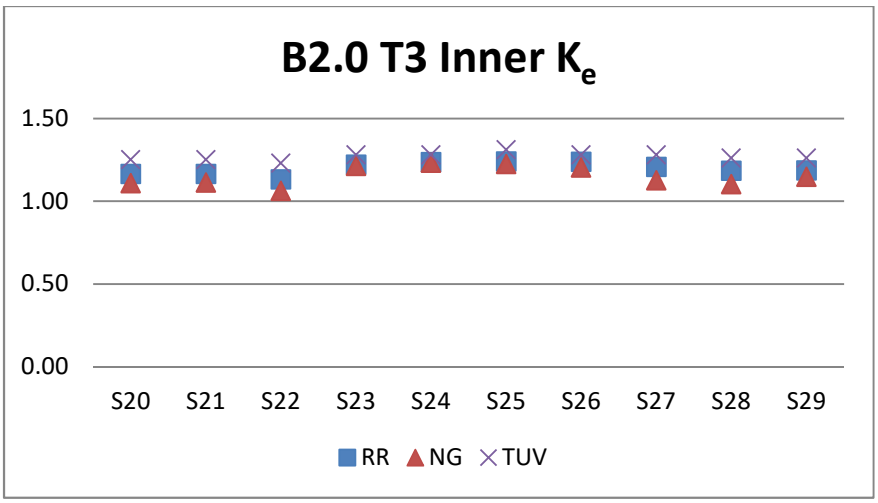

Figure 59. Benchmark 2.1 T3 inner K_e

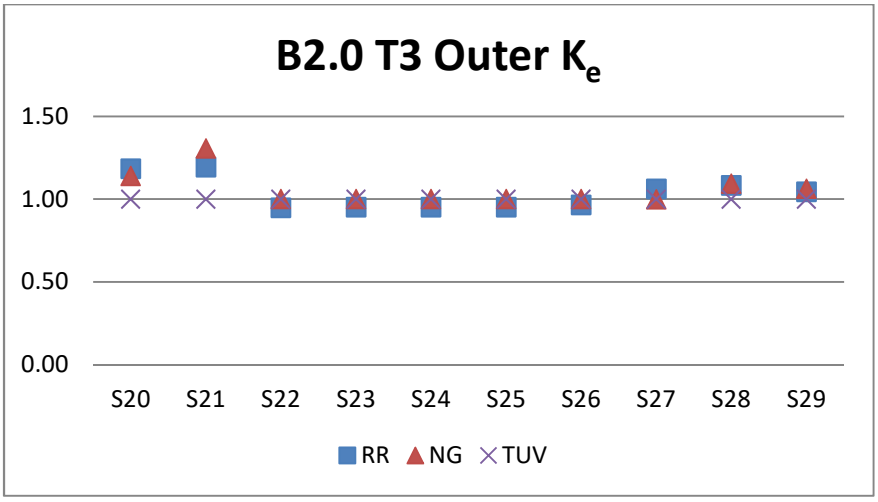

Figure 60. Benchmark 2.1 T3 outer K_e

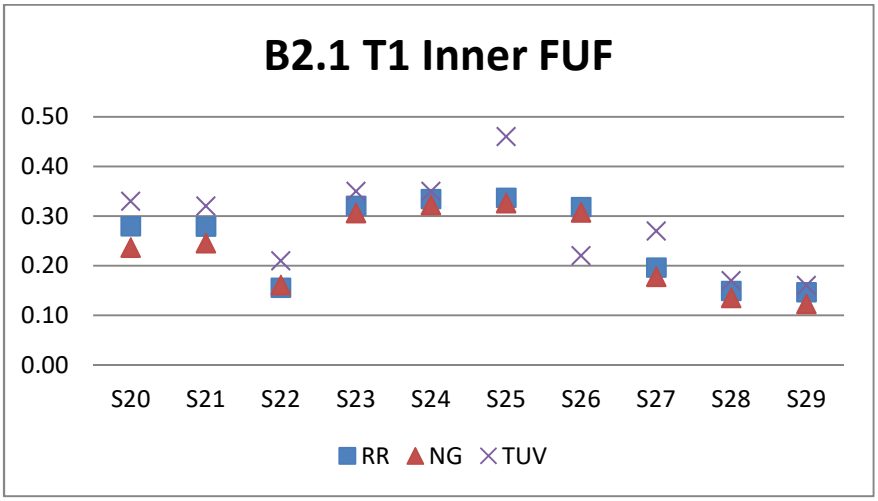

Figure 61. Benchmark 2.1 T1 inner FUF

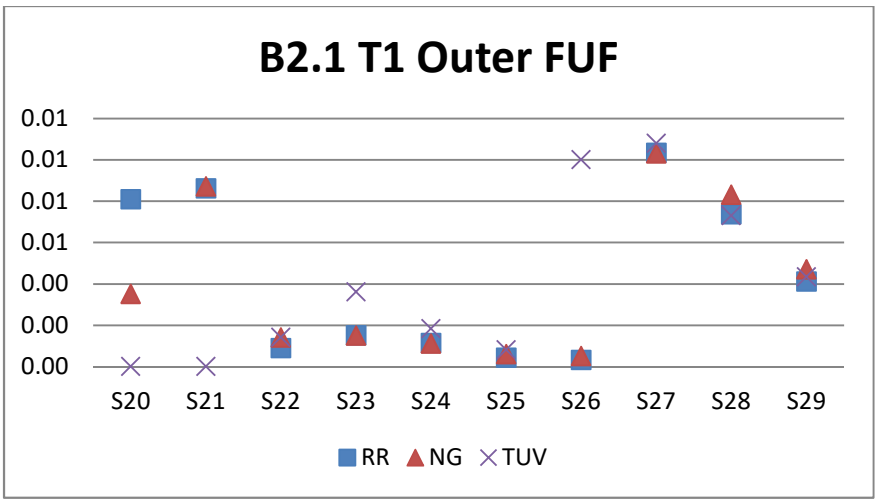

Figure 62. Benchmark 2.1 T1 outer FUF

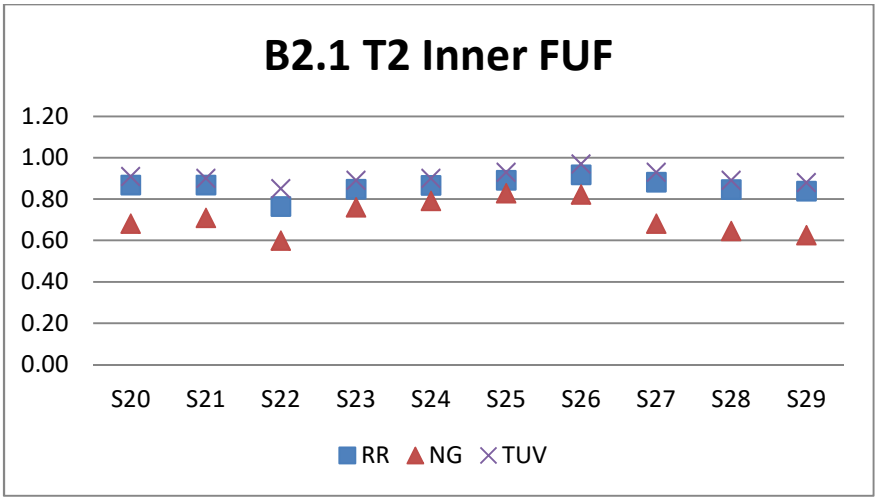

Figure 63. Benchmark 2.1 T2 inner FUF

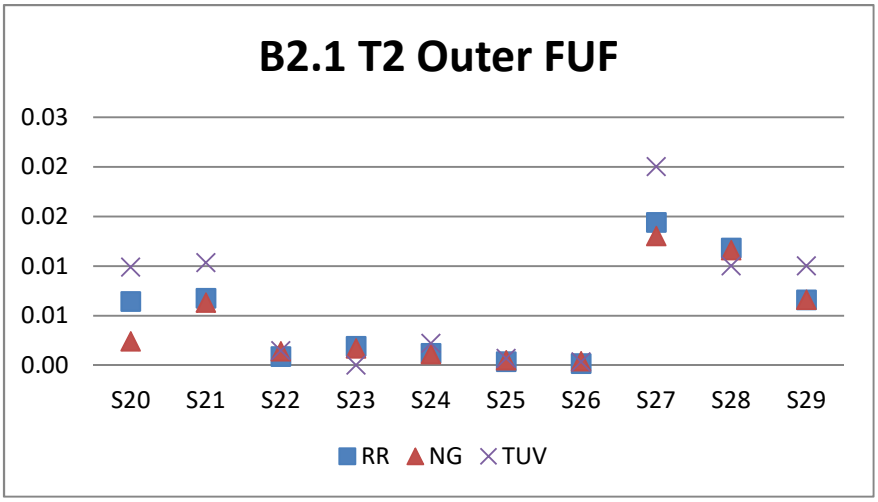

Figure 64. Benchmark 2.1 T2 outer FUF

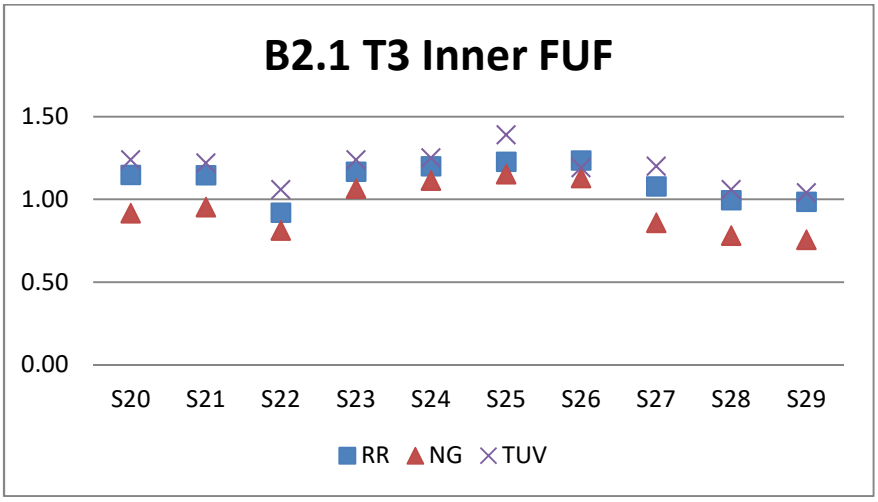

Figure 65. Benchmark 2.1 T3 inner FUF

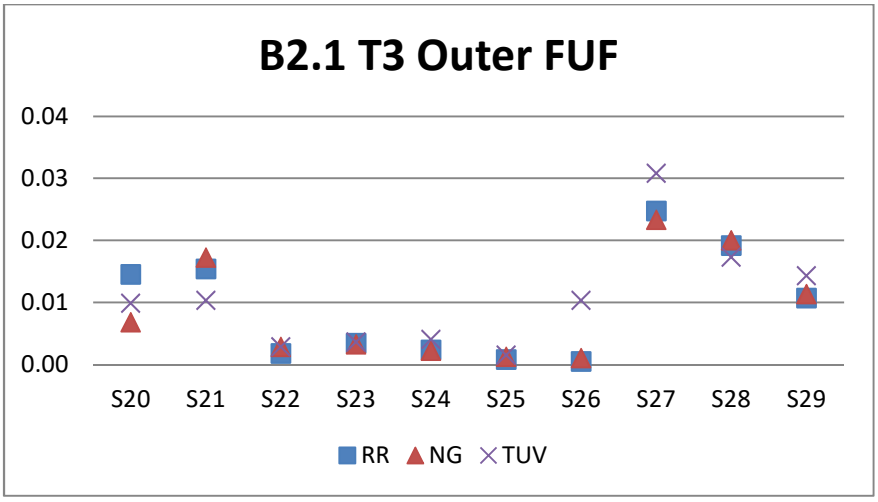

Figure 66. Benchmark 2.1 T3 outer FUF

Table 15. Benchmark 2.1 - Elastic-plastic equivalent strain range

	Assessment Location	Elastic-Plastic Strain Range ($\Delta\varepsilon_{ep}$)					
		Inner			Outer		
		Rolls-Royce	Naval Group	TUV	Rolls-Royce	Naval Group	TUV
Transient 1	S29	0.89%	0.82%	0.92%	0.29%	0.30%	0.30%
	S28	0.89%	0.83%	0.94%	0.35%	0.35%	0.35%
	S27	0.99%	0.93%	1.14%	0.38%	0.37%	0.39%
	S26	1.22%	1.16%	1.04%	0.16%	0.15%	0.38%
	S25	1.25%	1.20%	1.43%	0.17%	0.17%	0.19%
	S24	1.24%	1.19%	1.27%	0.21%	0.21%	0.23%
	S23	1.22%	1.17%	1.27%	0.22%	0.22%	0.28%
	S22	0.91%	0.83%	1.02%	0.20%	0.19%	0.22%
	S21	1.15%	1.09%	1.22%	0.37%	0.36%	N/A
	S20	1.15%	1.06%	1.24%	0.36%	0.25%	N/A
	Assessment Location	Elastic-Plastic Strain Range ($\Delta\varepsilon_{ep}$)					
		Inner			Outer		
		Rolls-Royce	Naval Group	TUV	Rolls-Royce	Naval Group	TUV
Transient 2	S29	0.78%	0.70%	0.79%	0.19%	0.19%	0.21%
	S28	0.78%	0.71%	0.80%	0.22%	0.22%	0.21%
	S27	0.79%	0.72%	0.81%	0.23%	0.23%	0.26%
	S26	0.81%	0.77%	0.82%	0.11%	0.12%	0.11%
	S25	0.80%	0.77%	0.81%	0.12%	0.12%	0.13%
	S24	0.79%	0.76%	0.80%	0.14%	0.14%	0.15%
	S23	0.78%	0.75%	0.80%	0.15%	0.15%	N/A
	S22	0.75%	0.69%	0.78%	0.13%	0.14%	0.14%
	S21	0.79%	0.73%	0.80%	0.19%	0.19%	0.21%
	S20	0.79%	0.72%	0.80%	0.19%	0.16%	0.21%

Table 16. Benchmark 2.1 - FE-derived plasticity correction factor (K_e)

	Assessment Location	FE-Derived K_e Factor					
		Inner			Outer		
		Rolls-Royce	Naval Group	TUV	Rolls-Royce	Naval Group	TUV
Transient 1	S29	1.185	1.112	1.260	1.042	1.060	1.000
	S28	1.183	1.102	1.260	1.079	1.092	1.000
	S27	1.205	1.124	1.280	1.059	0.997	1.000
	S26	1.238	1.202	1.280	0.963	1.000	1.000
	S25	1.239	1.224	1.310	0.922	1.000	1.000
	S24	1.236	1.232	1.280	0.944	1.000	1.000
	S23	1.220	1.211	1.280	0.939	1.000	1.000
	S22	1.077	1.000	1.230	0.937	1.000	1.000
	S21	1.163	1.111	1.250	1.180	1.209	1.000
	S20	1.163	1.108	1.250	1.174	1.059	1.000
	Assessment Location	FE-Derived K_e Factor					
		Inner			Outer		
		Rolls-Royce	Naval Group	TUV	Rolls-Royce	Naval Group	TUV
Transient 2	S29	1.176	1.077	1.190	0.938	1.000	1.000
	S28	1.177	1.075	1.190	0.956	1.000	1.000
	S27	1.174	1.078	1.190	0.954	1.000	1.000
	S26	1.152	1.114	1.180	0.965	1.000	1.000
	S25	1.145	1.131	1.170	0.953	1.000	1.000
	S24	1.140	1.120	1.160	0.953	1.000	1.000
	S23	1.136	1.112	1.160	0.953	1.000	1.000
	S22	1.132	1.000	1.160	0.949	1.000	1.000
	S21	1.140	1.081	1.160	0.943	1.000	1.000
	S20	1.140	1.083	1.160	0.942	1.000	1.000

Table 17. Benchmark 2.0 - Fatigue usage factor (FUF)

	Assessment Location	Fatigue Usage Factor (FUF)					
		Inner			Outer		
		Rolls-Royce	Naval Group	TUV	Rolls-Royce	Naval Group	TUV
Transient 1	S29	0.147	0.123	0.160	0.0041	0.0047	0.0043
	S28	0.149	0.135	0.170	0.0074	0.0083	0.0073
	S27	0.197	0.178	0.270	0.0103	0.0103	0.0108
	S26	0.318	0.308	0.220	0.0003	0.0005	0.0100
	S25	0.337	0.326	0.460	0.0004	0.0006	0.0008
	S24	0.335	0.322	0.350	0.0011	0.0011	0.0018
	S23	0.321	0.306	0.350	0.0015	0.0015	0.0036
	S22	0.156	0.161	0.210	0.0009	0.0014	0.0014
	S21	0.279	0.245	0.320	0.0086	0.0087	0.0000
	S20	0.280	0.236	0.330	0.0081	0.0035	0.0000
	Assessment Location	Fatigue Usage Factor (FUF)					
		Inner			Outer		
		Rolls-Royce	Naval Group	TUV	Rolls-Royce	Naval Group	TUV
Transient 2	S29	0.838	0.624	0.880	0.0066	0.0066	0.0100
	S28	0.846	0.645	0.890	0.0118	0.0116	0.0100
	S27	0.882	0.680	0.930	0.0144	0.0130	0.0200
	S26	0.916	0.822	0.970	0.0002	0.0004	0.0003
	S25	0.891	0.827	0.930	0.0004	0.0005	0.0007
	S24	0.867	0.791	0.900	0.0012	0.0011	0.0022
	S23	0.848	0.759	0.890	0.0019	0.0017	0.0000
	S22	0.764	0.599	0.850	0.0009	0.0014	0.0015
	S21	0.867	0.708	0.900	0.0068	0.0063	0.0103
	S20	0.868	0.680	0.910	0.0064	0.0024	0.0099
	Assessment Location	Fatigue Usage Factor (FUF)					
		Inner			Outer		
		Rolls-Royce	Naval Group	TUV	Rolls-Royce	Naval Group	TUV
Transient 1+2	S29	0.985	0.7555	1.040	0.0107	0.0113	0.0143
	S28	0.996	0.7799	1.060	0.0192	0.02	0.0173
	S27	1.079	0.8577	1.200	0.0247	0.0233	0.0308
	S26	1.234	1.129	1.190	0.0005	0.001	0.0103
	S25	1.228	1.1524	1.390	0.0008	0.0012	0.0015
	S24	1.201	1.1128	1.250	0.0024	0.0022	0.0041
	S23	1.168	1.0649	1.240	0.0034	0.0032	0.0036
	S22	0.920	0.8114	1.060	0.0018	0.0028	0.0029
	S21	1.146	0.9533	1.220	0.0154	0.0172	0.0103
	S20	1.147	0.9164	1.240	0.0145	0.0068	0.0099

4. Conclusions

Following an initial comparison of non-linear analysis design rules in nuclear mechanical codes and standards [1], two non-linear problems were specified for two typical nuclear components [2]. The first benchmark problem was based on a large class 1 low alloy steel vessel nozzle under pressure and piping loads where the aim was to analyze elastic stress, plastic collapse, plastic instability and local failure. The second benchmark problem was based on a class 1 reinforced stainless steel piping tee under cyclic pressure and thermal loads to perform fatigue assessment.

These benchmark problems have been analyzed by 10 international participants from China, France, Germany, India, Russia, South Korea, the UK and USA at various levels.

The first benchmark is defined in five parts (1.0 Elastic Codified Approach, 1.1 Plastic Collapse and Local Failure, 1.2 Plastic Instability, 1.3 Piping Load Effect and 1.4 3D Effects).

In the elastic codified approach (Benchmark 1.0), there is a good agreement of predicted membrane and combined stresses in the vessel and main coolant line outside of transition areas. The largest discrepancies are in inclined sections corresponding to the transitions from the vessel to the nozzle and from the nozzle reinforcement to the pipe, respectively. Differences also originate from the type of element, mesh refinement used in the model and the way stresses have been linearized, particularly bending stress. Variations in bending stress are believed to primarily come from the way bending stress values have been derived. There is also a need to discuss the limits of the approach to analyze a 3D geometry using a 2D model.

In Benchmark 1.1, plastic collapse values are obtained using three methods. There is a good agreement in the values of the limit load pressure predicted by the participants based on the yield stress. All results lie within 5% margin. The limit loads predicted by the other two methods (double slope and max 0.5% strain) show similar trends. It is clear from the results that the limit load is primarily influenced by the FEA method used in the simulation. It should be noted that the limit loads estimated based on strain criterion depend on the location where strain is being monitored.

Benchmark 1.2 focused on plastic instability predictions under pressure load based on flow stress, 5% strain and 10% strain. As expected, the results indicate that the 10% strain criteria give higher plastic instability load compared to those predicted by the 5% strain limit. It should be noted that strain-based criteria are influenced by the location of the strain. Another factor that influences the results is the value of the yield stress used to calculate the flow stress. Since the value of the flow stress is less than the stress at 5% strain, the flow stress criteria predicts the lowest plastic instability load and is a function of the material characteristic represented by the stress-strain curve.

The fourth part on pipe load effects (Benchmark 1.3) has not added much value to the non-linear analysis methods. For the exercise to be meaningful, a higher piping load, potentially including bending, should have been specified.

The fifth part (Benchmark 1.4) has shown that the assumptions made to represent a real 3D geometry as a 2D axisymmetric geometry are pessimistic. Higher and more realistic limit loads can be obtained if real 3D geometry is modelled. It can be concluded that the 3D model has confirmed that the limit loads and plastic instability loads obtained from the 2D model are within 10% margin.

The second benchmark problem was focused on fatigue assessment and was done in two parts (2.0 Codified Elastic Fatigue and 2.1 Simplified Non-Linear Analysis). In this benchmark, two quantities are derived, the plasticity correction factor, K_e, and fatigue usage factor (FUF) at the inner and outer surface at various locations using methods specified in ASME III and RCC-M.

For the codified elastic fatigue assessment (Benchmark 2.0), two transients were specified. Generally, there is good agreement of the trend in the K_e and FUF results calculated for both transients. Some differences in the K_e and FUF results were observed which could be due to the way stresses are resolved with respect to a cylindrical coordinate system defined locally to the section.

Benchmark 2.1 was aimed at applying simplified methods of elastic-plastic FEA to take account of plasticity in evaluating fatigue life. This benchmark has highlighted an important difference between ASME III and RCC-M. The consensus amongst participants was that the highest K_e and FUFs according to ASME III occur in the branch pipe and main coolant line. Comparatively, the nozzle experiences less damage according to ASME III. In contrast, two participants found that the highest K_e and FUF according to RCC-M are at the nozzle crotch corner. The reason for this is due to the effect of the pressure drop, which contributes to a higher mechanical stress intensity range at this location, which must be addressed explicitly in RCC-M calculations. However, it was recognized that significant differences could arise in the RCC-M fatigue results for Transient 2 depending on analyst assumptions, which are highlighted in the report. The method used to account for fluctuating mechanical loads in RCC-M calculations can also have a significant effect. A number of FEA assumptions were considered as having potential effects on the fatigue analysis results. The choice of linearization method may also have an influence on the results. Neither ASME III nor RCC-M provide explicit guidance on stress linearization and it is left to the judgement of the analyst.

It is acknowledged that whilst the stress ranges calculated by the participants were similar overall, even minor differences can have a significant ‘knock-on effect’ for downstream fatigue calculations. The reason for this is twofold. Firstly, it is due to the high non-linearity of the design fatigue curve in the low-cycle regime, where even a small difference in stress amplitude can result in a rather large difference in fatigue usage; secondly, slight differences in the stress intensity range may lead to potentially large differences in K_e which can also have a dramatic effect on the fatigue usage. A major source of difference between the K_e and FUF values reported by participants was due to the difference in the selection of the two distinct pairs of time points corresponding to their respective maxima and minima. A second major source of difference identified by the results for Transient 2 arose due to the methodology adopted for calculating the mechanical and thermal stress ranges in accordance with RCC-M.

Finally, a further comment raised by participants concerned the application of an alternative ASME III K_e factor, which, at the time of writing, has received approval from the

ASME Board on Nuclear Codes and Standards for publication as an ASME Section III Code Case (Record 17-225). There was interest to observe how this new K_e factor, denoted K_e*, compared with the other K_e factors analysed. One participant investigated this difference for Benchmark 2.0 and found that overall, the new ASME III K_e* factor exhibited a similar trend to the RCC-M K_e factor, and accordingly the FUFs calculated using this new approach are much more closely aligned to RCC-M compared with the standard ASME III, Appendix XIII-3450 approach. However, there were found to be some cases where more significant divergence can occur between K_e* and the RCC-M K_e factors, which can arise depending on the loading condition.

Close assessment of the differences in the results submitted by the participants has identified three main causes:

- Modelling assumptions made by the analysts;
- Analysis and assessment methods adopted by the analysts;
- Differences in the design code rules.

However, it should be noted that the benchmark problem conditions would be more severe than the challenges faced by industry practitioners in real-life scenarios, since the two benchmark problems were designed to identify areas the where consensus appears to be emerging and areas where further discussions are needed to harmonize the non-linear analysis approach used by the analysts.

These international non-linear benchmark exercises have identified several areas where no guidance is provided in the design codes for the analysts who use FEA to analyze and assess a design. It is proposed to provide recommendations in the following areas in Part 3 of this report series:

Static Analysis

- How local stresses normal to the section are resolved.
- Selection and definition of the positioning of the section where stresses are being evaluated.
- More detailed guidelines about linearization procedures. Which stress components should be linearized and how?
- Define the limits of the approach to analyze a 3D geometry with a 2D model.
- Selection of the location where strain is being monitored for strain-based methods to estimate limit loads.
- How to derive a true stress-strain curve from material data.
- Selecting the value of flow stress to be used for limit load.
- When to use full 3D analysis.
- How to reduce pessimism in limit load prediction by use of full 3D geometry.

Cyclic Analysis

- Combination of transients for fatigue assessment particularly the selection of time points to obtain the maxima and minima of the stress range.
- Methodology for obtaining peak stress range under combined cyclic mechanical and thermal loading.
- Accuracy of adopted cyclic stress-strain curve (bi-linear, multi-linear, etc.).
- Choice of cyclic yield strength, S_y^c, and constitutive model for elastic-plastic FEA.
- Choice of equivalent strain range for characterisation of fatigue damage.
- Calculation of K_e factor based on FEA results.
- Calculation of FUF.

References

[1] CORDEL Mechanical Codes and Standards Task Force (MCSTF), Non-Linear Analysis Design Rules, Part 1: Code Comparison, February 2017

[2] CORDEL Mechanical Codes and Standards Task Force (MCSTF), Non-Linear Analysis Design Rules, Part 2a: Specification of Benchmarks on Nozzles under Pressure, Thermal, and Piping Loads, July 2019.

[3] ASME Boiler & Pressure Vessel Code, Section III - Rules for Construction of Nuclear Facilities Components, Subsection NB Class 1 Components, ASME, 2017 Edition.

[4] RCC-M: Design and Construction Rules for Mechanical Components of PWR Nuclear Island, AFCEN, 2015 Edition.

[5] ASME Boiler & Pressure Vessel Code,, Section VIII, Division 2: Alternative Rules, ASME, 2015 Edition

[6] JL Hechmer and GL Hollinger, “3D Stress Criteria Guidelines For Application,” WRC Bulletin 429, Welding Research Council, 1998

[7] ASME, Record 17-225, Proposed Code Case, Alternative Rules for Simplified Elastic-Plastic Analysis in Section III (forthcoming).

World Nuclear Association
Tower House
10 Southampton Street
London WC2E 7HA
United Kingdom

+44 (0)20 7451 1520
www.world-nuclear.org
info@world-nuclear.org